Toxin Reviews

ISSN: (Print) (Online) Journal homepage: https://www.tandfonline.com/loi/itxr20

# Hydrogeochemical characterization, multi-exposure deterministic and probabilistic health hazard evaluation in groundwater in parts of Northern India

Herojeet Rajkumar, Pradeep K. Naik, Gagandeep Singh & Madhuri Rishi

**To cite this article:** Herojeet Rajkumar, Pradeep K. Naik, Gagandeep Singh & Madhuri Rishi (2022): Hydrogeochemical characterization, multi-exposure deterministic and probabilistic health hazard evaluation in groundwater in parts of Northern India, Toxin Reviews, DOI: 10.1080/15569543.2022.2080222

**To link to this article:** https://doi.org/10.1080/15569543.2022.2080222



Published online: 30 May 2022.

TOXIN REVIEWS
https://doi.org/10.1080/15569543.2022.2080222



RESEARCH ARTICLE

# Hydrogeochemical characterization, multi-exposure deterministic and probabilistic health hazard evaluation in groundwater in parts of Northern India

Herojeet Rajkumar[a], Pradeep K. Naik[b], Gagandeep Singh[c] and Madhuri Rishi[d]

[a]Department of Environment Studies, Post Graduate Government College, Chandigarh, India; [b]Rajiv Gandhi National Ground Water Training & Research Institute, Raipur, Chhattisgarh, India; [c]Punjab Biodiversity Board, Chandigarh, India; [d]Department of Environmental Studies, Panjab University, Chandigarh, India

**ABSTRACT**

This work attempts to identify the latent factors controlling the hydrogeochemistry and assess the groundwater quality and associated health risks in the intermontane valley of Nalagarh in the sub-Himalayan zone in northern India. Analytical results of 64 groundwater samples, 32 each collected during pre monsoon and post monsoon seasons show contrasting results for their major chemical constituents. During pre monsoon period, only 3% of the samples exceed their permissible limits for pH, EC, TH and $Mg^{2+}$, while during post monsoon period, different parameters, such as TH, $Mg^{2+}$ and $K^{+}$, exceed their limits by 9, 16, and 3%, respectively. Gibbs and Piper diagrams reveal that groundwater chemistry is mainly controlled by water-sediment (alluvial) interaction. Geochemical signatures and saturation index (*SI*) further indicate that the weathering and dissolution of silicate, calcite and dolomite minerals mainly contributed to dominance of $Ca^{2+}$, $Mg^{2+}$ and $HCO_3^-$ ions in the aquifers. Monte Carlo simulation ascertains non-carcinogenic health risks due to $NO_3^-$ and $F^-$ in different sub-population groups. Deterministic and probabilistic estimates of these parameters via ingestion and dermal routes confirm their percentage hazard toxicity in the order infants (58.38; 39.62%) >children (15.62; 15.85%) >teens (6.25; 2.73%) >adults (6.25; 1.90%) for pre monsoon. The hazard toxicity for deterministic study implies only on infants (9.38%), whereas, the probabilistic simulation extracted the health risk on infants (6.57%), and children (0.58%) during post monsoon. Minor populations with their lower body weights are more vulnerable to groundwater pollution due to greater consumption of liquid diet. Therefore, treated groundwater is strongly recommended to mitigate health morbidities linked with the non-cancerous risks.

**ARTICLE HISTORY**
Received 24 October 2021
Revised 22 April 2022
Accepted 17 May 2022

**KEYWORDS**
Groundwater quality; geochemical signature; saturation index; health risk; Monte Carlo simulation sensitivity analysis

## 1. Introduction

Groundwater is an indispensable freshwater resource used for multiple activities supporting about two-thirds of the global population (Wang *et al.* 2020, Selvam *et al.* 2021, Gao *et al.* 2022). More than one billion people living in countries like India, China, Pakistan, Bangladesh, and Nepal heavily rely on groundwater for their needs (Gleeson *et al.* 2012, Li *et al.* 2014, Adimalla and Wu 2019). India's rapid groundwater development pace fulfills the water demand by ∼50% urban and semi-urban drinking water, and ∼85% rural domestic and irrigation supply (Jain and Vaid 2018, Singh *et al.* 2020b). The quality of groundwater plays a vital role in the socio-economic development, agricultural sector, and importance to the human health perspective (Li *et al.* 2019a, Aravinthasamy *et al.* 2021). The alluvial aquifers developed along the foothills slope are more propensities to contamination due to numerous human interventions, namely urbanization, agricultural expansions, mining, and industrial activities (EPA 1993, Naik *et al.* 2008, Herojeet *et al.* 2016, Radfard *et al.* 2019). The groundwater quality of alluvial foothill zones is significant because of the strongly influenced by hydro-geological and physiographic setup, climatic and anthropogenic factors (Rajkumar *et al.* 2020). Some of the natural inputs impacting the groundwater chemistry are ion exchange, weathering and dissolution of rock minerals, litho-water interaction, and atmospheric transports (Li *et al.* 2018a, b, Karunanidhi *et al.* 2020;

**CONTACT** Herojeet Rajkumar herojeet.rk@gmail.com Department of Environment Studies, Post Graduate Government College, Sector-11, Chandigarh, India

Supplemental data for this article can be accessed online at https://doi.org/10.1080/15569543.2022.2080222.

Singh *et al.* 2020a). Therefore, groundwater quality monitoring is necessary for sustainable water management to prevent over-exploitation and quality deterioration (Herojeet *et al.* 2013, Dolma *et al.* 2015, Tiwari *et al.* 2018).

In India, groundwater is often used directly for different purposes without proper treatment due to lack of awareness, and necessary economic and technological limitations (Madhav *et al.* 2018, Rao *et al.* 2021). Such practice of groundwater consumption may easily expose to various contaminants viz, inorganic, organic, heavy metals, and other pollutants are a significant threat to human health (Ghaderpoori *et al.* 2018, Aravinthasamy *et al.* 2021). The continuous exposures to fluoride ($F^-$) and nitrates ($NO_3^-$)-containing groundwater are vulnerable to non-carcinogenic health risks on the local populace (Rao *et al.* 2021). The low content of $F^-$ in drinking water is beneficial for the formation and development of teeth, and skeleton. Nevertheless, the concentration above the guideline limit (1.5 mg/L) is harmful to human health, causing dental fluorosis, osteoporosis, arthritis, neurotoxicity, and thyroid (WHO 2011, BIS 2012). The sources and occurrence of $F^-$ in an alluvial aquifer are very complex and uncertain due to numerous point and non-point inputs, geochemical, and pedogenesis processes compared to aquifer developed in fractured hard rocks bearing $F^-$ minerals (Kim *et al.* 2012, Adimalla and Venkatayogi 2017). In India, 26 States among its 29 States witness high $F^-$ levels in groundwater, posing the risk of endemic fluorosis to ~66 million individuals (~25 million <18 years) in 250 districts (Narsimha and Rajitha 2018).

$NO_3^-$ contaminant in groundwater is a worldwide environmental concern due to its unique properties, such as high movability and solubility rate, stable oxidative state in water and associated health risks (WHO 2008, Zhai *et al.* 2017, He et al. 2022a). Groundwater pollution due to $NO_3^-$ is widely reported in various countries, namely in Loess plateau, Northwest China (Li *et al.* 2019b), Matanza-Riachuelo River Basin, Argentina (Ceballos *et al.* 2021), Weining plain and Yinchuan plain, Northwest China (He *et al.* 2022a, 2022b), Donsheng district, Inner Mongolia (Feng *et al.* 2020), Gorveh-Dehgelan, Western Iran (Rahmati *et al.* 2015), Catalan Region, Spain (Carrey *et al.* 2021) and Guanzhong plain, China (Wang and Li 2022). In India, ~118 million people consume water with $NO_3^-$ content 45–100 mg/L, and ~108 million people drink water containing $NO_3^-$ level >100 mg/L (Rai 2003, Sangwan *et al.* 2021). Anthropogenic activities, such as application of N-chemical fertilizers (Huang *et al.* 2011), excreta from animals farm (Minet *et al.* 2017, Zhang *et al.* 2018), urban runoff (Lapworth *et al.* 2017), landfill leachate (Rao *et al.* 2021), wastewater irrigation (Elisante and Muzuka 2017) and discharge of untreated municipal, sewage and industrial effluents (Herojeet *et al.* 2016, He et al. 2022a), are the leading causes for $NO_3^-$ loads. The acute toxicity of $NO_3^-$ is often encountered even though the concentration level for drinking water is below 45 mg/L in infants (<1 year) and children by "blue baby syndrome" (Skold et al. 2011, BIS 2012). Long-term exposure to $NO_3^-$ has chronic effects on human health, such as non-Hodgkin lymphoma, nitrosamines, and multiple sclerosis (Fabro *et al.* 2015, Wongsanit *et al.* 2015). Therefore, the health hazard risks of such ions are still concerns to infants and children even at low concentration due to exposure dose, sensitivity and weak tolerance limit (Adimalla and Qian 2019).

Human health risk assessment (HHRA) is an equation developed by USEPA, that deals with quantitative hazard risk appraisal on human health concerning specific chemical contents in water (Qiu and Gui 2019, Li *et al.* 2021). Most of the researchers have studied the non-carcinogenic HHRA for $F^-$ and $NO_3^-$ in India using deterministic method (Adimalla *et al.* 2019, Adimalla and Qian 2019, Kumar *et al.* 2019, Karunanidhi *et al.* 2020, Rao *et al.* 2021, Sangwan *et al.* 2021, Selvam *et al.* 2021). The implementation of deterministic method is conservative in risk analysis due to the fixed assigned value of input variables rather than the range of random values of each variable (Saha *et al.* 2017). The variables used in deterministic model normally vary with respect to time, places, climatic conditions (ingestion rate, bathing frequency), types of receptors (different age groups, exposure frequency and body weight) and parameter concentrations (Liu *et al.* 2022). Thus, the uncertainty associated with input variables randomness of the deterministic approach may overestimate or underestimate the risk assessment, thereby diluting the study's objective. Many researchers proposed other health risk models considering the traditional method limitation, namely gray system theory, fuzzy mathematical theory and probabilistic theory (Wang 2004). Gray system theory is a developing model with ambiguous principles due to addition of numerous concepts and methods as per the worker's discretion. Bilgil (2021) suggested that gray system theory may sometimes yield unacceptable prediction errors. Also, this model is applicable for short-term predictions with limited sample sizes and partial information of the problems (Liu *et al.* 2022). Fuzzy theory deals with the things that lacks clear boundaries of the approach, and probabilistic statistical model is applied to study the probability approximation of events affected by input random factors (Zhou 2017). Probabilistic approach, namely, Monte Carlo Simulation (MCS), is considered the logically superior and promising stochastic method to appraise HHRA (Giri *et al.* 2020; Emenike *et al.* 2019). MCS approach caters to quantitative variability and reduces uncertainties by providing more accurate and prospective risk assessment outcomes than the conventional deterministic method.

Nalagarh represents the inter-monte valley situated in Himachal Pradesh, Northern India. During the past decades, the serene valley of Nalagarh turned into an industrial hub, thereby discharging enormous untreated effluents causing pollution on perennial and ephemeral streams and soil. Presently, groundwater is the primary source for domestic, irrigation, and industrial purposes in the study area. Due to rapid industrialization, the large-scale groundwater development witnessed a declining water level of the valley (CGWB (Central Ground Water Board) 2018). Therefore, groundwater depletion and their pollution vulnerability are the major threat in the study area. Various latent factors influence groundwater evolution, and complex processes that can be interpreted using multiple appraisal approaches, viz, interionic interpolations, geochemical characterization and thermodynamic modeling, and statistical techniques (Singh *et al.* 2020a, Sangwan *et al.* 2021). The present study is carried out to characterize the groundwater quality for drinking purposes, geochemical evolution, and non-carcinogenic HHRA of groundwater viz, ingestion, and dermal route using deterministic and probabilistic approaches in parts of Northern India.

### 1.1. Study area

Nalagarh valley, a narrow stretch of low lying area carved in the tertiary formations, covering an area of about 250 km$^2$ with a population of about 254,390 people and decadal growth rate of 13.8% is selected for the present study (Figure 1). The valley is delineated by the lesser Siwalik Hills in the northeast (NE), and River Sirsa drained at the foothill of the outer Siwalik Hills in the southwest (SW). Agriculture and forest land cover classes are the dominant land use type in the study area covering about 6.67 and 36.10% of the total geographical area, respectively (Figure 2). Nearly 4.62% of the study area is covered by water bodies that include rivers and streams. Approximately 15 and 5 km$^2$ of geographical areas are under settlement and industrial land use classes, respectively, forming around 5.4% of the study area. In the last decades, the State government has emphasized industrialization in the hilly ecosystem terrain by granting numerous special incentives (Kamaldeep *et al.* 2011). The industrial region in Nalagarh valley named as Baddi-Barotirwala-Nalagarh (BBN) witnessed 12 different industrial categories with a maximum number (∼70%) of large and medium scale industrial units, which is a pollution threat to water resources (GoHP (Government of Himachal Pradesh) 2012, Rajkumar *et al.* 2020). As per a report by the BBN Authority in 2007, as many as 72% of industrial units do not install their effluent treatment plants (ETPs). These units openly discharge their untreated effluents to the open channels and agricultural lands increasing susceptibility to groundwater pollution. Numerous ephemeral and perennial streams, often loaded with untreated industrial effluents, and sewage wastewater, flow through the BBN industrial region and join the Sirsa River (CGWB (Central Ground Water Board) 2007, 2008). Therefore, Sirsa River and its tributaries cannot often fulfill the quality water demand of the study area as they are heavily contaminated due to pollutant discharges from the various sources (Rajkumar *et al.* 2019). All water requirements of the valley, including those for public water supply, industrial and irrigational supply, are met by groundwater resources only (CGWB 2013).

### 1.2. Geology and hydrogeology

Nalagarh is a northwest-southeast (NW-SE) trending intermontane valley in the lesser Himalayas in northern India (Figure 1). Flanked by the Siwaliks of Tertiary Age, it forms a relatively low lying narrow strip of about 5–7 km. Its topography and geology has been described by Rajkumar (2019, 2020). Lesser Siwalik Hills with a maximum elevation of 1150 meter above mean sea level (m amsl) form the NE flank while the outer Siwalik Hills with an elevation of about 500 m amsl form the SW flank. The formation of Nalagarh valley is linked to the last phase of upheaval of the Himalayas as it runs parallel to the main strike direction of the Siwalik formations. While pre-Holocene and Holocene deposits form the granular alluvial soils in Nalagarh valley, the common rock types encountered are sandstone, quartzite, limestone, phyllite, slate and shale. These rocks are well-jointed, factured and crushed at places. Nalagarh and Sirsa thrusts are the two major NW-SE trending tectonic zones with the Surajpur Fault paving the path for the Sirsa River (Khan 1970).

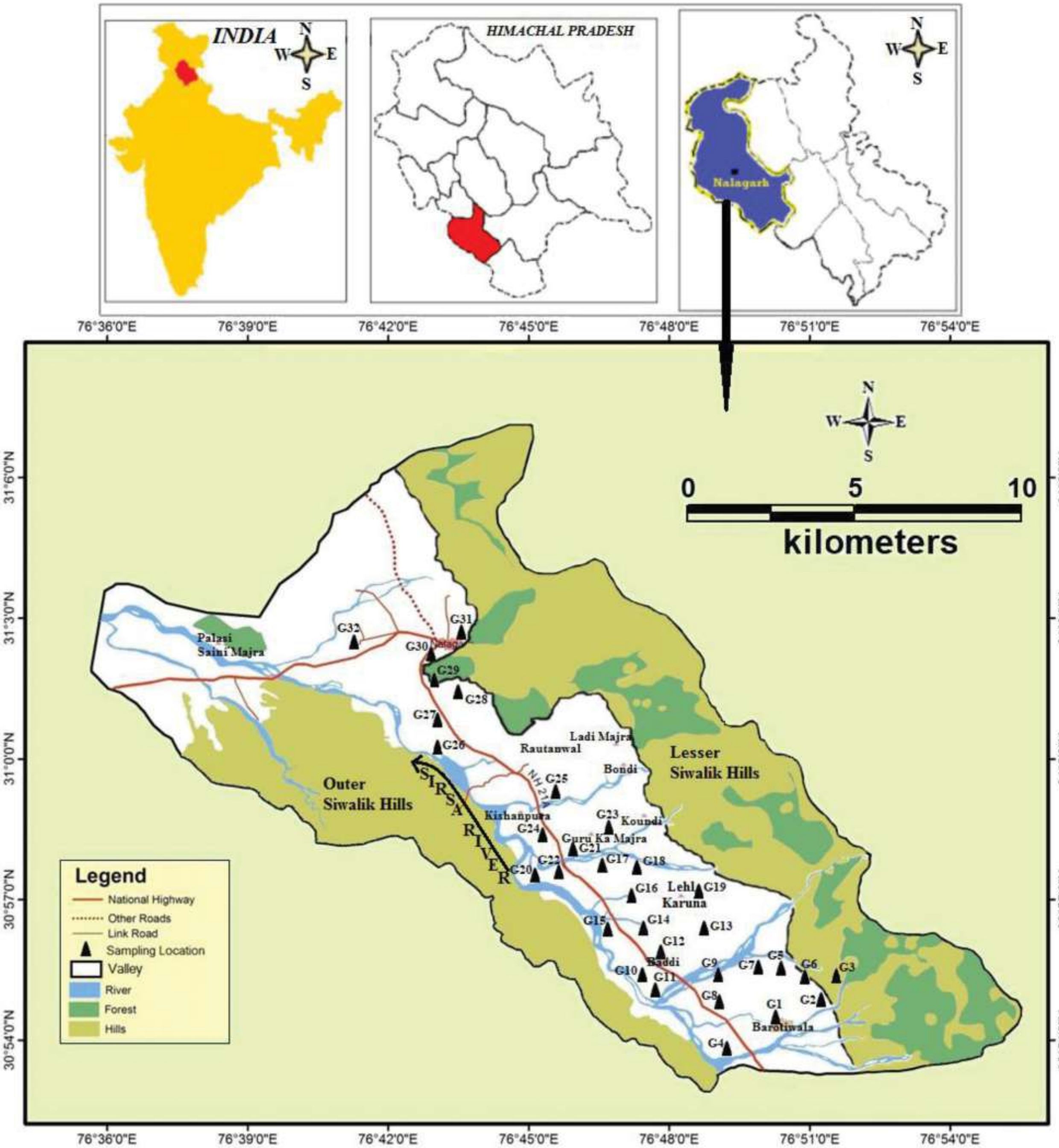


**Figure 1.** Location of the Nalagarh valley, Himachal Pradesh, India.

Groundwater in the valley occurs in pervious unconsolidated alluvial formations under both phreatic and confined conditions (CGWB (Central Ground Water Board) 2018). Groundwater levels are shallower in the main valley portions with depth to water levels (DTW) varying between near zero and 10 meter below ground level (mbgl) during premonsoon period (May 2014). As the surface slope rises toward the hills, DTW starts becoming deeper (Rajkumar *et al.* 2020). Various types of groundwater structures encountered are tubewells of varying depths, 4–60 m deep dugwells and dug-cum-borewells. As per CGWB (Central Ground Water Board) (2008), general yields of these wells go upto 10 liters per second (lps), but wells tapping a granular zone at 25–30 m depth have yields upto 30 lps. Semi-confined aquifers are tapped by about 65–120 m deep tubewells.

The primary source of groundwater recharge in the area is South-West monsoon (July–September) that causes about 83% of rainfall with an annual average of 1129.3 mm in about 64 rainy days. Other recharge sources are the seepage from irrigation water, abandoned mine pits and influent perennial and ephemeral

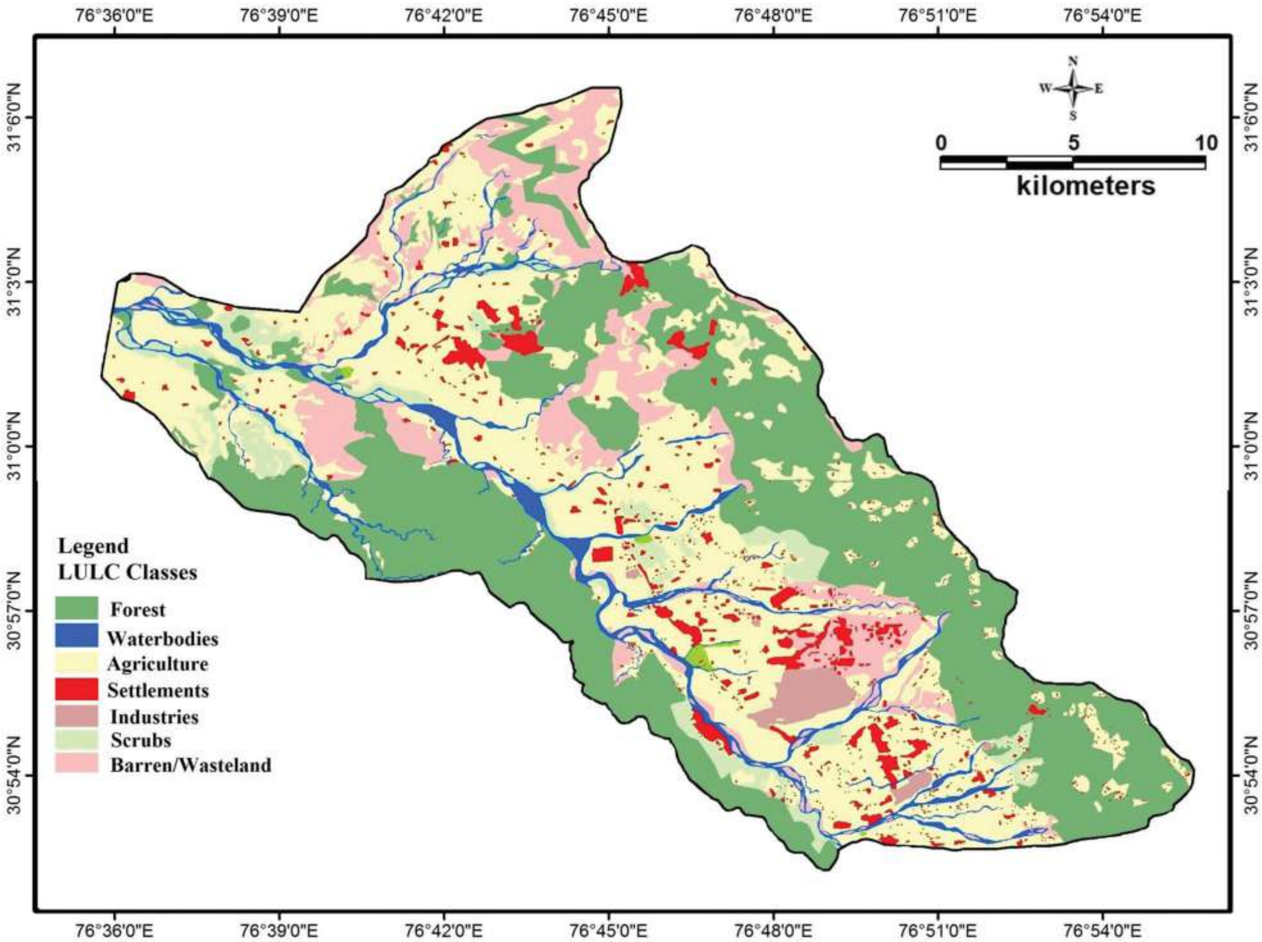


Figure 2. Landuse Landcover (LULC) of the study area.

streams. The dendritic drainage pattern favors infiltration and percolation of a large quantity of water into the porous and highly permeable valley-fill deposits. The groundwater discharge mainly occurs naturally through evapotranspiration and effluent seepages into the major streams and artificially through groundwater extraction by dugwells, tube wells and dug-cum-borewells for various uses.

The groundwater movement follows the surface topography and is generally toward the SW direction corresponding to the orientation of the valley slope (Figure 3). The water table elevation ranges from 265 to 465 m amsl. The groundwater flow along the SW slope intersects the Sirsa riverbed and those of many other tributaries to maintain their perennial flow (CGWB (Central Ground Water Board) 2008).

## 2. Materials and methods

### 2.1. Sampling and laboratory investigation

Groundwater samples were collected from 32 different locations including 18 sites from the pheratic aquifers and 14 sites from semi-confined aquifers in the study area (Figure 1) during both pre and post monsoon seasons (May and October, 2012) using the Global Position System. Thus, a total of 64 groundwater samples were collected for chemical analysis. Plastic bottles (HDPE) of 1000 ml capacity were prewashed with 10% nitric acid ($HNO_3$) and soaked with double deionized water. To obtain fresh samples, flushing the groundwater source for about 10–15 min will remove the stagnant water stored in pipes. Bottles were again rinsed 2–3 times with the water to be collected to preserve and maintain the original water characteristics. Parameters, namely pH, and electrical conductivity (EC) were examined at the sampling sites itself using portable multiparameter (Hanna HI98194) and total dissolved solids (TDS) were calculated using the formula (TDS = EC * 0.64) immediately on the spot. Each sampling site has collected one pair of groundwater samples using Whatman filter paper (0.45 μm) to remove suspended particulate matter. Samples were preserved by acidifying (pH ~2 with $HNO_3$) and kept at a temperature of 4 °C for the analysis of major cations. The standard protocol (APHA 2005) was followed for the investigation of major cations ($Ca^{2+}$, $Mg^{2+}$,

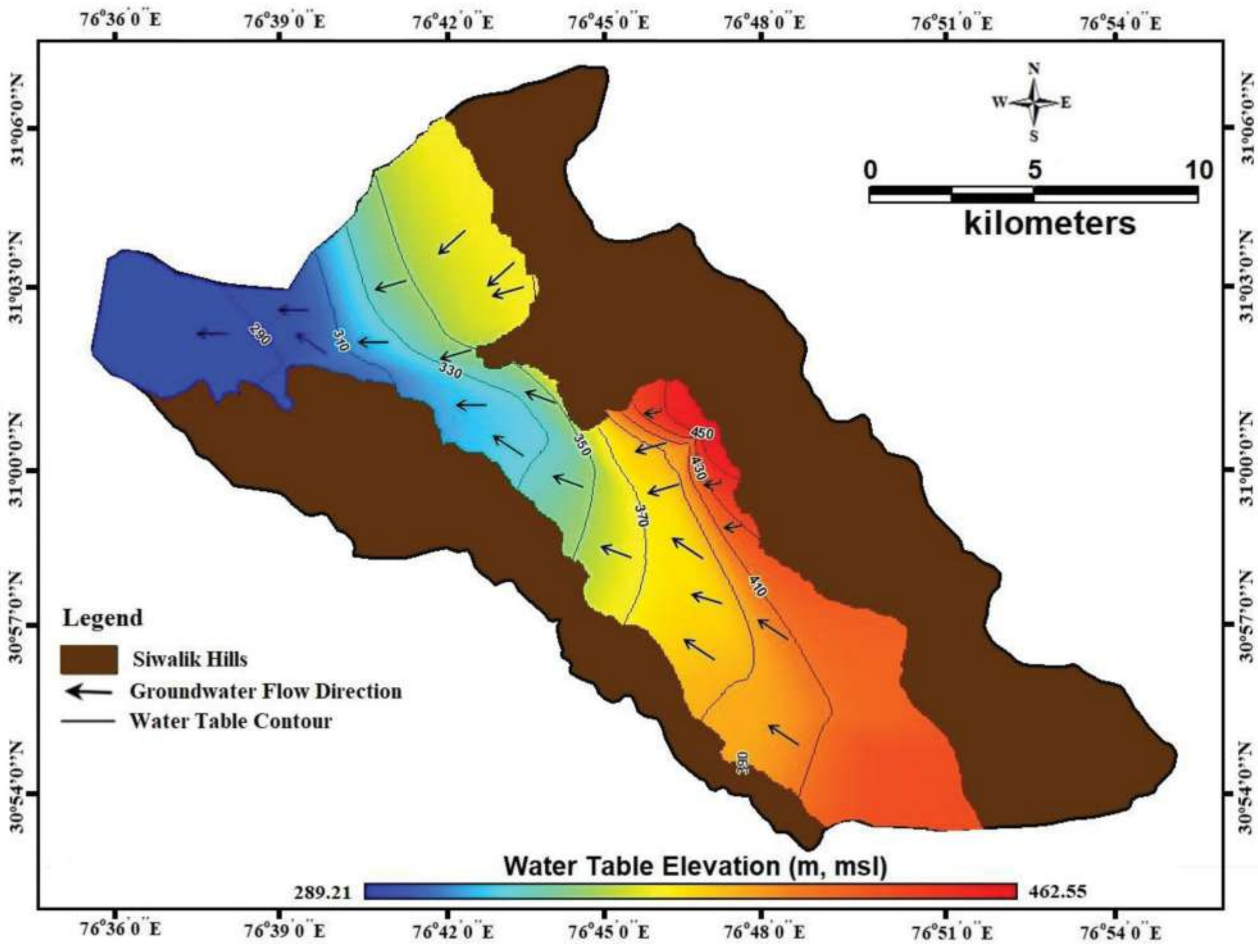


Figure 3. Groundwater flow direction in the Nalagarh valley, Himachal Pradesh.

$Na^+$, and $K^+$) and major anions ($HCO_3^-$, $Cl^-$, $SO_4^{2-}$, $F^-$, and $NO_3^-$). Merck-GR grade chemicals and reagents were used to prepare the chemical solutions using double deionized water. All the glassware and apparatus were soaked with 10% hydrochloric acid (HCl) for one day and cleaned with double deionized water. Blank samples were prepared from the stock solutions of each parameter for instrumental calibration. The accuracy of analyze datasets was computed using the charge balance error (CBE) equation (Equation 1), and each sample value was less than their acceptable limit (±5%) (Hounslow 2018).

$$CBE\% = \frac{\sum(Cations)meq/L - \sum(Anions)meq/L}{\sum(Cations)meq/L + \sum(Anions)meq/L} \times 100 \tag{1}$$

Mapinfo Professional 6.5 is used for the map digitization, and Originpro 18 and MS Office 2010 are used for various graphical interpolations and statistical calculations. RockWorks15 and PHREEQC Version 3 are used for geochemical modeling in groundwater.

## 2.2. Deterministic and probabilistic human health risk analysis

Risk analysis is an essential mathematical model to evaluate the negative effect on human health due to harmful contaminants in water sources over a specific time period (USEPA (US Environmental Protection Agency) 1989, 1992). Human health risk assessment (HHRA) guidelines give four necessary steps: (i) hazard identification, (ii) exposure assessment, (iii) dose-response assessment, and (iv) risk characterization (Luo *et al.* 2012, Ma *et al.* 2016).

i. *Hazard identification*: The hazard level is evaluated for chemical contaminants due to their high mobility and adverse toxic effects when exposed to humans over a specific time (USEPA (US Environmental Protection Agency) 2004, Guleria and Chakma 2021). Interaction with local people in the study area confirmed their sole dependence on groundwater for drinking, domestic and agricultural purposes. The potential human health risk associated with a low concentration of contaminants in groundwater through various pathways may be negligible. Although, the degree of adverse health effects on different age groups may be concerned even at low concentrations because of the physiological variation, organs developmental process, age factor, and specific chemical tolerance on the human body. Therefore, the adverse toxicity health risk may be relatively intensified with increased contaminants in water.

ii. *Exposure assessment*: The exposure of HHRA is estimated through three different pathways, namely, direct oral ingestion as drinking water, inhalation of water droplets or aerosol through mouth and nose, and dermal contact to exposed skin (USEPA (US Environmental Protection Agency) 1989). Among the three exposure pathways, direct oral ingestion and dermal contact are the significant and shared pathways for chemical exposure to the human body (Singh and Kumar 2017, Emenike *et al.* 2019). In the present study, $F^-$ and $NO_3^-$ are the target parameters, and their average daily dose (*ADD*) is used to determine the non-carcinogenic HHRA via, direct ingestion ($ADD_{ingestion}$) and dermal contact ($ADD_{dermal}$) through bathing and other domestic activities using the Equations 2 and 3 (USEPA (US Environmental Protection Agency) 2011). The assessment of *ADD* is computed on four different subpopulation groups, namely; infants (<1 year), children (1–11 years), teens (11–18 years), and adults (>18 years), respectively, due to their behavioral and physiological attributes.

$$ADD_{ingestion} = \frac{C_M \times IR_w \times EF_r \times ED}{BW \times AT_r} \tag{2}$$

$$ADD_{dermal} = \frac{C_M \times SA \times K_p \times EF_r \times ED \times ET \times CF}{BW \times AT_r} \tag{3}$$

iii. *Dose-response assessment*: The quantification of exposure hazard level of any potentially toxic non-carcinogenic chemical on human health is examined by dose-response assessment (Lee *et al.* 2006, Guleria and Chakma 2021). Reference dose (*RfD*) is defined as the permissible guideline limit set by USEPA, above which the designated population is susceptible to toxic substances (Ma *et al.* 2016). The reference dose of dermal skin adsorption ($RfD_d$) for many contaminants is not available in IRIS database (https://www.epa.gov/iris). However, USEPA (US Environmental Protection Agency) (2002a) suggested a formula to derive the dermal reference dose ($RfD_d$) from the oral reference dose ($RfD_i$) using the following Equation 4.

$$RfD_d = RfD_i \times ABS_i \tag{4}$$

Where $ABS_i$ is the gastrointestinal absorption factor (unitless) of the i^th^ chemical parameter. The $ABS_i$ value of $NO_3^-$ and $F^-$ is 1 (USDHAHS 2017, USEPA (US Environmental Protection Agency) 2002b). Therefore, *RfD* of $NO_3^-$ and $F^-$ for ingestion and dermal route are 1.6 mg/kg per day and 0.06 mg/kg per day, respectively (USEPA (US Environmental Protection Agency) 2002a, 2012; Ali *et al.* 2021).

iv. Risk characterization: Risk characterization of non-carcinogenic chemical parameter is assessed through hazard quotient (*HQ*) and hazard index (*HI*). *HQ* is the ratio of exposure assessment of health risk (*ADD*) for different age groups and their respective reference dose (*RfD*) of target parameter at each pathway (USDHAHS 2017, USEPA (US Environmental Protection Agency) 2004) and is computed by using Equations 5 and 6. *HQ* is unitless value. If *HQ* value exceeds the threshold limit 1, the potential adverse health effect is associated with a particular exposure pathway.

$$HQ_{ingestion} = \frac{ADD_{ingestion}}{RfD_i} \tag{5}$$

$$HQ_{dermal} = \frac{ADD_{dermal}}{RfD_d} \tag{6}$$

Furthermore, *HI* is the combined non-carcinogenic risk, i.e. the summation of *HQ* of each assessment subpopulation group for different chemical parameters and exposure pathways (Saha *et al.* 2017). *HI* is unitless and calculated using Equations 7 and 8.

$$HI_{ingestion} = \sum_{i=1}^{n} HQ(F^-)_{ingestion} + \sum_{i=1}^{n} HQ(NO_3^-)_{ingestion} \tag{7}$$

$$HI_{dermal} = \sum_{i=1}^{n} HQ(F^-)_{dermal} + \sum_{i=1}^{n} HQ(NO_3^-)_{dermal} \tag{8}$$

$$THI = \sum_{i=1}^{n} HI_{ingestion} + \sum_{i=1}^{n} HI_{dermal} \tag{9}$$

Where *THI* is the total hazard index, and *i* indicate the exposure pathway considered in the study (Equation 9). $HI > 1$ indicates the potential non-carcinogenic toxicity in the specified age group (USEPA (US Environmental Protection Agency) 2004).

In this study, deterministic and probabilistic risk analysis methods are employed to ascertain the uncertainty and sensitivity of health risk assessment. The deterministic approach used the simple mathematical formula recommended by USEPA, where the input variables are fixed values for different exposure routes (Lin *et al.* 2016). The output risk results generated from this method are only point or single value that neglects the quantitative variability and uncertainty in the applied model's input variables (USEPA (US Environmental Protection Agency) 1997, Rajasekhar *et al.* 2018). Therefore, the deterministic approach of HHRA cannot cater to the absolute or holistic scenario of risk assessment for the inclusive member of population interest due to differences in person-to-person characteristics and dynamism prevailing in the environment. USEPA (US Environmental Protection Agency) (1997) suggested probabilistic techniques as an alternative and viable statistical application offering a sound methodology and new research dimension that provides more credible information and authentic scientific output for the risk analysis.

Probabilistic techniques, namely, MCS are purposely applied to analyze the input variables that reduce the associated uncertainty of various pathways in risk assessment. MCS is a computer software application configuring a statistical distribution array in the form of probabilistic approximation of a mathematical equation to generate more corroborates reproducibility results. MCS is performed using Oracle Crystal Ball software version (11.1.2.4.850). Each input parameter is arranged according to their corresponding minimum, maximum, mean, and standard deviation (SD) values to assign the best-fitted statistics distribution types and establish their probability distribution functions (PDFs) (USEPA (US Environmental Protection Agency) 1997). The input parameters such as ingestion rate ($IR_w$), exposure frequency ($EF$), expose skin surface area ($SA$), exposure time ($ET$), and body weight ($BW$) are employed 10,000 repetitions of oral ingestion and dermal contact route for each subpopulation category. Thus, the numerical stability of MCS is obtained at 10,000 permutations for $HQ$, $HI$, and $THI$ (Ganyaglo *et al.* 2019, Jamal *et al.* 2019). The sensitivity analysis is also employed to extract the significant input variables impacting the outcome of risk simulation model. The target parameters, i.e. $F^-$ and $NO_3^-$, are defined by the auto-select to best-fitted probability distribution pattern based on their concentration values, and their goodness of fit (GoF) statistics outcome are presented in Table 1. The values and types of distribution of various variables for ingestion and dermal pathways for the deterministic and probabilistic risk assessment are provided in supplementary Table S1.

## 3. Results and discussions

### 3.1. General groundwater characteristics

The basic statistical information that includes minimum, maximum, mean ± SD values of analyzed groundwater parameters and compliance with drinking water standards of WHO (2011) and BIS (2012) is presented in Table 2. The analytical results of pH indicate the alkaline nature of groundwater and ranges from 7.2 to 8.7 (mean ± SD value 7.6 ± 0.4) and 7.0 − 8.1 (mean ± SD value 7.4 ± 0.2) during the investigational period i.e. pre and post monsoon seasons. All the groundwater samples have pH values within their recommended limit (6.5 − 8.5) of BIS (2012) and WHO (2011), except for one sample (S8) during pre monsoon season (Table 2). EC values vary between 500 and 1513 µS/cm and 443 and 1348 µS/cm during pre and post monsoon seasons, respectively, and well within the guideline value (1500 µS/cm) of WHO (2011); except for one sample (S31) during pre monsoon season (Table 2). TDS values varies between 324 and 992 mg/L (pre monsoon) and 284 and 875 mg/L (post monsoon), whereas, TH concentration ranges from 206 to 622 mg/L and 186 to 772 mg/L during the investigational period. The mean concentrations of EC and TDS are slightly more in pre monsoon season (909 µS/cm and 589 mg/L) than during the post monsoon period (808 µS/cm and 522 mg/L). This may be due to groundwater draft before the onset of

**Table 1.** Best fitted probability distribution for nitrate and fluoride parameters and goodness of fit (GoF) outcomes.

| Parameters | Distribution types and their parameter values | Anderson-Darling Test | Anderson-Darling Test (*p* value) | Kolmogorov-Smirnov Test | Kolmogorov-Smirnov Test (*p* value) | Chi-Square Test | Chi-Square Test (*p* value) |
|---|---|---|---|---|---|---|---|
| Premonsoon | | | | | | | |
| Fluoride | Lognormal (Location = 0.00, Mean = 0.22, Std. Dev = 0.16) | 0.5585 | 0.068 | 0.1215 | 0.152 | 7.00 | 0.030 |
| Nitrate | Beta (Minimum = 0.87, Maximum = 66.03, Alpha = 1.58292) | 0.2620 | – | 0.0852 | – | 2.1250 | 0.145 |
| Postmonsoon | | | | | | | |
| Fluoride | Gamma (Location = 0.05, Scale = 0.10, Shape = 1.53618 | 0.2977 | 0.824 | 0.0874 | 0.944 | 2.8750 | 0.238 |
| Nitrate | Exponential (Rate = 0.26) | 0.6470 | 0.314 | 0.1387 | 0.312 | 5.8750 | 0.209 |

**Table 2.** Statistical analyses of groundwater samples in Nalagarh valley, Himachal Pradesh, India.

| | BIS (2012) Standards | | Pre monsoon | | | | Post monsoon | | | | |
|---|---|---|---|---|---|---|---|---|---|---|---|
| | | | | | % of samples (numbers) above BIS (2012) Standards | | | | % of samples (numbers) above BIS (2012) Standards | | |
| Parameter | AL | PL | Range | Mean ± SD | AL | PL | Range | Mean ± SD | AL | PL | Analytical method |
| Physical parameters | | | | | | | | | | | |
| pH | 6.5-8.5 | | 7.2–8.7 | 7.6 ± 0.4 | 3.0 (1) | | 7.0–8.1 | 7.41 ± 0.23 | NIL | | pH/EC/TDS meter |
| EC | 1500* | | 500–1513 | 909 ± 248 | 3.0 (1) | | 443–1348 | 808 ± 271 | NIL | | pH/EC/TDS meter |
| TDS | 500 | 2000 | 324–992 | 589 ± 185 | 65.6 (21) | NIL | 284–875 | 522 ± 175 | 46.9 (15) | NIL | TDS = EC* 0.64 |
| TH | 200 | 600 | 206–622 | 306 ± 87 | 96.9 (31) | 3.0 (1) | 186–772 | 381 ± 155 | 84.4 (27) | 9.4 (3) | Titration with EDTA using Eriochrome Black T as indicator |
| Major cations | | | | | | | | | | | |
| $Mg^{2+}$ | 30 | 100 | 20.6–137.2 | 56.7 ± 21.7 | 90.6 (29) | 3.0 (1) | 31.7–172.8 | 73.4 ± 36.7 | 84.4 (27) | 15.6 (5) | Titration with EDTA as titrant and eriochrome black T as indicator) |
| $Ca^{2+}$ | 75 | 200 | 35.3–157.3 | 74.0 ± 28.2 | 40.6 (13) | NIL | 27.6–138.6 | 79.8 ± 31.1 | 53.1 (17) | NIL | Titration with EDTA using Murexide as indicator |
| $Na^+$ | 200* | | 12.0 – 99.9 | 35.0 ± 22.0 | NIL | | 9.1–62.5 | 29.5 ± 12.1 | NIL | | Flame photometric |
| $K^+$ | 12* | | 0.9 – 8.8 | 2.4 ± 1.5 | NIL | | 0.4–19.0 | 2.1 ± 3.2 | 3.0 (1) | | Flame photometric |
| Major anions | | | | | | | | | | | |
| $HCO_3^-$ | 500* | | 60.0 – 196.0 | 118.9 ± 28.7 | NIL | | 62.0–204.0 | 129.6 ± 28.4 | NIL | | Titrimetric method using standard $H_2SO_4$ with phenolphthalein and methyl orange as an indicator |
| $Cl^-$ | 250 | 1000 | 2.8–36.2 | 15.2 ± 9.0 | NIL | NIL | 3.9 – 39.8 | 15.8 ± 9.6 | NIL | NIL | Titration with AgNO3 using potassium dichromate as indicator |
| $SO_4^{2-}$ | 200 | 400 | 10.0–27.0 | 13.2 ± 3.3 | NIL | NIL | 9.7 – 26.5 | 13.3 ± 4.0 | NIL | NIL | Spectrophotometer (using $BaCl_2$ as conditioning agent) |
| $F^-$ | 1 | 1.5 | 0.06–1.20 | 0.22 ± 0.21 | 3.0 (1) | NIL | 0.05 – 0.50 | 0.20 ± 0.11 | NIL | NIL | Spectrophotometer (SPADNS Method) |
| $NO_3^-$ | 45 | | 2.6 – 38.8 | 14.6 ± 9.2 | NIL | | BDL–18.9 | 3.9 ± 4.3 | NIL | | Spectrophotometer (using phenol disulfonic acid) |

*Note*: Unit in mg/L, Except EC (µS/cm) and pH and BDL means below detectable limit. AL and PL specifies the acceptable limit and the permissible limit.
*Since BIS (2012) does not specify any guideline value, WHO (2011) guideline value has been considered.

**Table 3.** Groundwater classification based on TDS, TH, $F^-$ and $NO_3^-$.

| Parameters | Range | Classification | No of samples exceeding allowable limits | |
|---|---|---|---|---|
| | | | Pre monsoon | Post monsoon |
| TDS (mg/L) | <1000 | Fresh | 32 | 32 |
| (Freeze and Cherry 1979) | 1000–10,000 | Brackish | Nil | Nil |
| | 10,000–100,000 | Saline | Nil | Nil |
| | >100,000 | Brine | Nil | Nil |
| TH (mg/L) | <75 | Soft | Nil | Nil |
| (Sawyer and McCarty 1967) | 75–150 | Moderately hard | Nil | Nil |
| | 150–300 | Hard | 18 | 16 |
| | >300 | Very hard | 14 | 16 |
| $NO_3^-$ (mg/L) | <45 | Low risk (suitable for drinking) | 32 | 32 |
| (Adimalla *et al.* 2019 and Singh *et al.* 2020b) | 46 – 100 | High risk (not suitable for drinking) | Nil | Nil |
| | >100 | Very high risk (not suitable for drinking) | Nil | Nil |
| $F^-$ (mg/L) | <0.5 | Class 1 (dental Caries) | 31 | 32 |
| (Adimalla *et al.* 2019; Singh *et al.* 2020b) | 0.6 – 1.5 | Class 2 (required levels for human health) | 1 | Nil |
| | 1.6 – 2.0 | Class 3 (dental fluorosis) | Nil | Nil |
| | 2.1 – 3.0 | Class 4 (dental & skeletal fluorosis) | Nil | Nil |
| | >3.0 | Class 5 (leads to skeletal fluorosis) | Nil | Nil |

monsoon season, and enhancement of ion exchange processes for mineralization and salinity in the aquifers (Herojeet *et al.* 2016). The groundwater quality of the study area is classified into freshwater category i.e. TDS values <1000 mg/L as per Freeze and Cherry 1979 classification (Table 3). Sawyer and McCarty 1967 (Sawyer and McCarty 1967) classification based on TH values, all groundwater samples are categorized into hard to very hard water classes for both the seasons (Table 3). Further, the plot between TDS vs. TH infers that the groundwater is hard to very hard in nature during the investigational period (Figure S1). Continuous consumption of such water types may link to various cardiovascular diseases viz, urolithiasis, anencephaly, neurological problems, and muscle slackening (Kumar and Augustine 2021, Sangwan *et al.* 2021). TH mean value is more during post monsoon (381 mg/L) than pre monsoon (306 mg/L), as carbonate minerals (calcite, dolomite, sandstone) are readily dissolved in percolating slightly acidic rainwater during monsoon period and reverse ion exchange process (Zhou *et al.* 2020). Similarly, the average content of $Mg^{2+}$ and $Ca^{2+}$ ions are more in post monsoon than pre monsoon in the groundwater (Table 2). Thus, the high degree of hardness is often associated with the elevated concentration of $Mg^{2+}$ and $Ca^{2+}$ in the aquifer system (Herojeet *et al.* 2016). The relative abundance order of major ions in the groundwater of the study area are as follows; $Mg^{2+}>Ca^{2+}>Na^+>K^+$ and $HCO_3^->Cl^->SO_4^{2-}>NO_3^->F^-$ [Figure 4(a)].

### 3.2. Major ions chemistry

In groundwater, $Mg^{2+}$ content ranges from 20.6 to 137.2 mg/L with 56.7 ± 21.7 and 31.7 – 172.8 mg/L with 73.4 ± 36.7, respectively, during pre and post monsoon. 3% (pre monsoon) and 16% (post monsoon) samples are above the $Mg^{2+}$ permissible limit (100 mg/L) of BIS (2012) (Table 2). $Ca^{2+}$ concentration varies from 35.3 to 157.2 mg/L and 27.6 to 138.6 mg/L during pre and post monsoon, respectively. About 41% of groundwater samples in pre monsoon and 53% in post monsoon have $Ca^{2+}$ levels above the acceptable limit (75 mg/L) for drinking purposes (BIS 2012) (Table 2). Several geochemical processes like weathering of silicate minerals (plagioclase, amphiboles, pyroxenes) and magnesium bearing minerals (dolomite, sandstone) along with reverse ion exchange, and fertilizers applications may be the possible sources of $Ca^{2+}$ and $Mg^{2+}$ ions in the groundwater of the study area (Zhou *et al.* 2020, Singh *et al.* 2020b, Liu *et al.* 2021).

$Na^+$ concentration ranges from 12.0 to 99.9 mg/L in pre monsoon and 9.1 to 62.5 mg/L in post monsoon seasons. Higher mean value of 35.0 mg/L in pre monsoon season (Table 2) indicates ion exchange and silicate weathering processes (Gao *et al.* 2021). $K^+$ (the least dominant cation) content varies between 0.9 and 8.80 mg/L (pre monsoon) and 0.4 and 19.0 mg/L (post monsoon) in the study area. Only 3% of post monsoon samples have surpassed the $K^+$ guideline limit of 12 mg/L for drinking purposes (WHO 2011) with no significant variation in mean concentrations in both the seasons (Table 2).

$HCO_3^-$ is the most dominant ion among the anions and ranges from 60.0 to 196.0 mg/L (118.9 ± 28.7) and 62.0 to 204.0 mg/L (129.6 ± 28.4) during pre monsoon and post monsoon seasons, respectively. The mean concentration of $HCO_3^-$ ion in groundwater is slightly higher during post monsoon season (129.6 mg/L) compared to that of pre monsoon period (118.9 mg/L) indicating dissolution of silicate and carbonate

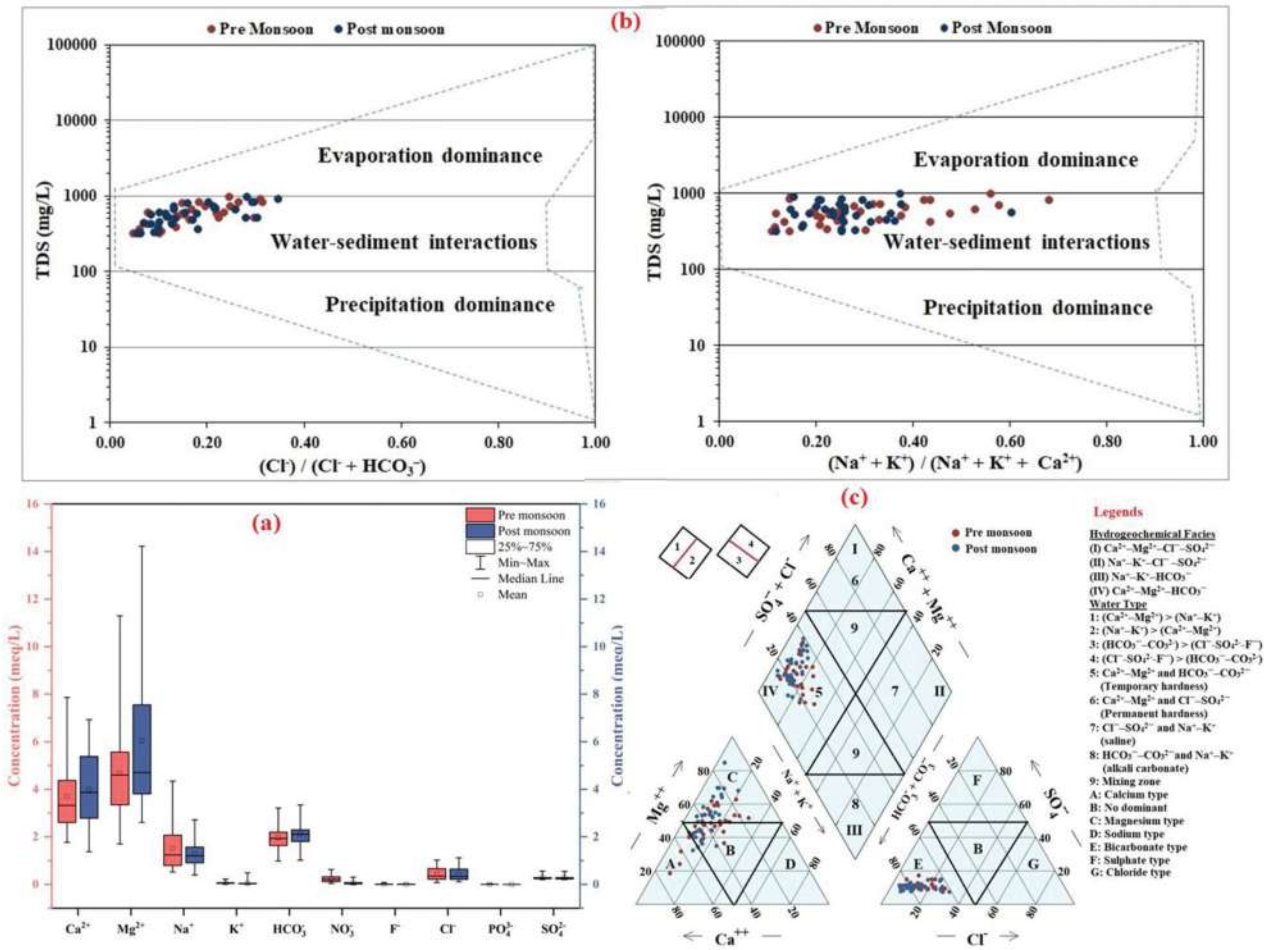


**Figure 4.** (a) Relative abundance order of major ions in groundwater samples, (b) Gibbs diagram representing the factor controlling groundwater chemistry, and (c) Piper diagram illustrating hydrochemical facies and water type.

minerals with the percolating rainwater during the monsoon. $Cl^-$ concentration varies from 2.8 to 36.2 mg/L and 3.9 to 39.8 mg/L during pre monsoon and post monsoon seasons, respectively. $SO_4^{2-}$ concentration ranges between 10.0 and 27.0 mg/L and 9.7 and 26.5 mg/L, respectively, during these seasons. The mean values of $Cl^-$ and $SO_4^{2-}$ ions in groundwater show no significant variation for both the seasons (Table 2). The parameters $HCO_3^-$, $Cl^-$ and $SO_4^{2-}$ are within the respective guideline limits prescribed by the BIS (2012) and WHO (2011) (Table 2).

### *3.3. Health concern parameters*

$F^-$ concentration varies from 0.06 to 1.20 mg/L with mean (0.22 mg/L) (pre monsoon), and 0.05 to 0.50 mg/L with mean (0.20 mg/L) (post monsoon) and within the permissible limit for human intake i.e. 1.5 mg/L (BIS 2012) (Table 2). Only 3% sample during pre monsoon is above the $F^-$ acceptable limit (1.0 mg/L) of BIS (2012). The groundwater classification based upon $F^-$ content by Adimalla *et al.* (2019) and Singh *et al.* (2020b) is summarized in Table 3. All groundwater samples for both seasons are categorized in class-I (<0.5 mg/L; conducive to dental caries), except one sample (S13 in the central part of the study area) during pre monsoon. $NO_3^-$ content in pre and post monsoon seasons ranges from 2.6 to 38.8 mg/L and below detection limit (BDL) to 18.9 mg/L respectively (Table 2) and within the guideline limit (45 mg/L) of BIS (2012). Table 3 shows that all groundwater samples are categorized into low risk $NO_3^-$ content class as per Adimalla *et al.* (2019) and Singh *et al.* (2020b). Analytical results revealed that few groundwater sampling locations mostly confined to the Baddi industrial region showed an elevated level of $NO_3^-$. Anthropogenic factors like municipal and industrial discharges, seepage from the septic tanks, and drainage channels are the contributing factors for $NO_3^-$ in the study area (Rao *et al.* 2012, Singh *et al.* 2019, Wang *et al.* 2021).

### 3.4. Hydrogeochemical processes

For a better understanding of the key mechanisms controlling aquifer chemistry, Gibbs diagrams (Gibbs 1970) are prepared to represent the relationship between the TDS and cation ratio i.e. $Na^+/(Na^+ + Ca^{2+})$ or anion ratio i.e. $Cl^-/(Cl^- + HCO_3^-)$. Figure 4(b) shows that all the groundwater samples are clustered on water-sediment interaction zone. Such interactive phenomena of water-alluvial sediment are mainly due to the dissolution and weathering of rock-forming minerals along with the cation exchange (direct and reverse) processes (Herojeet *et al.* 2013, Sidhu *et al.* 2013). The alluvial deposits are rich in silicate minerals along with secondary carbonate minerals like calcite [$CaCO_3$] and dolomite [$CaMg(CO_3)_2$] in the study area (CGWB (Central Ground Water Board) 2018). The weathering of these minerals determines the groundwater characteristic and the possible ions constituents in the groundwater (Rao 2017, Rao *et al.* 2021). Further, the Piper diagram (Piper 1944) is prepared to identify the hydrochemical facies and water types through the mixing effects between groundwater and aquifer minerals. All the groundwater samples belong to Zone IV during the investigational period, i.e. $Ca^{2+}$–$Mg^{2+}$–$HCO_3^-$ hydrochemical facies [Figure 4(c)]. The diamond field of Piper's diagram indicates that alkaline earth elements ($Ca^{2+}$–$Mg^{2+}$) exceed the alkalies elements ($Na^+$–$K^+$) and weak acids ($CO_3^{2-}$–$HCO_3^-$) exceed the strong acids ($SO_4^{2-}$–$Cl^-$), indicating thereby that the groundwater is dominated by $Ca^{2+}$, $Mg^{2+}$ and $HCO_3^-$ ions [Figure 2(c)]. Such water types are mainly attributed to carbonate-rich material dissolution within the aquifers as expressed in Equations 10–12 (Singh *et al.* 2019, Zhang *et al.* 2020, Keesari *et al.* 2021).

$$CaCO_3 + H_2CO_3 \leftrightarrow Ca^{2+} + 2HCO_3^- \tag{10}$$

$$CaMg(CO_3)_2 + 2H^+ \leftrightarrow CaCO_3 + Mg^{2+} + H_2CO_3 \tag{11}$$

$$CaSO_4 + CaMgCO_3 + 6H^+ \leftrightarrow CaCO_3 + Ca^{2+} + Mg^{2+} + SO_4^{2-} + H_2CO_3 \tag{12}$$

### 3.5. Geogenic weathering and ion exchange

Various interionic plots were prepared to understand the hydrogeochemical and chemical weathering processes in the aquifers. $Ca^{2+}/Mg^{2+}$ ratio was computed to determine the possible sources of $Ca^{2+}$ and $Mg^{2+}$ in the aquifer systems (Gao *et al.* 2022). In Figure 5(a), ~66% of groundwater samples during the investigational period are fall in $Ca^{2+}/Mg^{2+}$ ratio below 1, which indicates the dominance of dolomite dissolution over calcite dissolution in the study area (Mayo and Loucks 1995). Few samples (28% pre monsoon and 34% post monsoon) lie on or above $Ca^{2+}/Mg^{2+}$ ratio line 1 but less than 2, specifies the dissolution of both dolomite and calcite minerals. The remaining 6% samples during pre monsoon fall above $Ca^{2+}/Mg^{2+}$ ratio line 2, suggesting the effect of silicate minerals (Figure 5(a)). The plot between $Ca^{2+}+Mg^{2+}$ vs. $HCO_3^-+SO_4^{2-}$ shows all the groundwater samples are falling above the equiline (1:1), reflecting the carbonate weathering (calcite and dolomite) is largely affecting the aquifer chemistry (Figure 5(b)). The dominance of $Ca^{2+}$ and $Mg^{2+}$ over $HCO_3^-$ and $SO_4^{2-}$ may also be attributed to the reverse ion exchange process (as expressed in Equations (17) and (18) and carbonate weathering (Luo *et al.* 2021, Karunanidhi *et al.* 2021b). The bivariate plot of $Ca^{2+}+Mg^{2+}$ vs. Total Cations ($TZ^+$) shows all the samples are scattered between the equiline (1:1) and $Ca^{2+}+Mg^{2+} = 0.5\ TZ^+$ line (Figure 5(c)). It depicts the weathering of calc-silicate minerals (plagioclase, amphiboles) and carbonates (dolomite and calcite) is contributing $Ca^{2+}$ and $Mg^{2+}$ ions in the aquifer (Li *et al.* 2020). In the bivariate plot of $Ca^{2+}$ vs. $HCO_3^-$ (Figure 5(d)), very few samples (6% and 9%) fall below the equimolar line (1:1), whereas a large scatter of samples (93% and 91%) are falling above the equimolar line (1:1) during the investigational period. The plot $Mg^{2+}$ vs. $HCO_3^-$ (Figure 5(e)) indicates that 97 and 3% of samples fall above and below the equiline (1:1) for both seasons. These trends show the $Ca^{2+}$ and $Mg^{2+}$ are dominantly contributed from calcite and dolomite weathering and reverse ion exchange processes in the aquifer chemistry of the study area (Marghade *et al.* 2021, Selvam *et al.* 2021).

### 3.6. Mixed factors (geogenic and anthropogenic)

The bivariate plot between $Na^++K^+$ and $TZ^+$ (Figure 5(f)) infers that all the water samples are scattered below the equiline ($Na^++K^+ = 0.5TZ^+$). It implies the weathering of potash and silicate-containing minerals and anthropogenic inputs like the application of potash fertilizers and sewage wastewater which contributes mainly $Na^+$ and $K^+$ ions to the groundwater (Srinivasamoorthy *et al.* 2014, Rao *et al.* 2021). The dissolution of sodium bearing silicate minerals like albite (as expressed in Equation (13) and other soda plagioclase feldspars in the presence of $H_2CO_3$ acid (formed

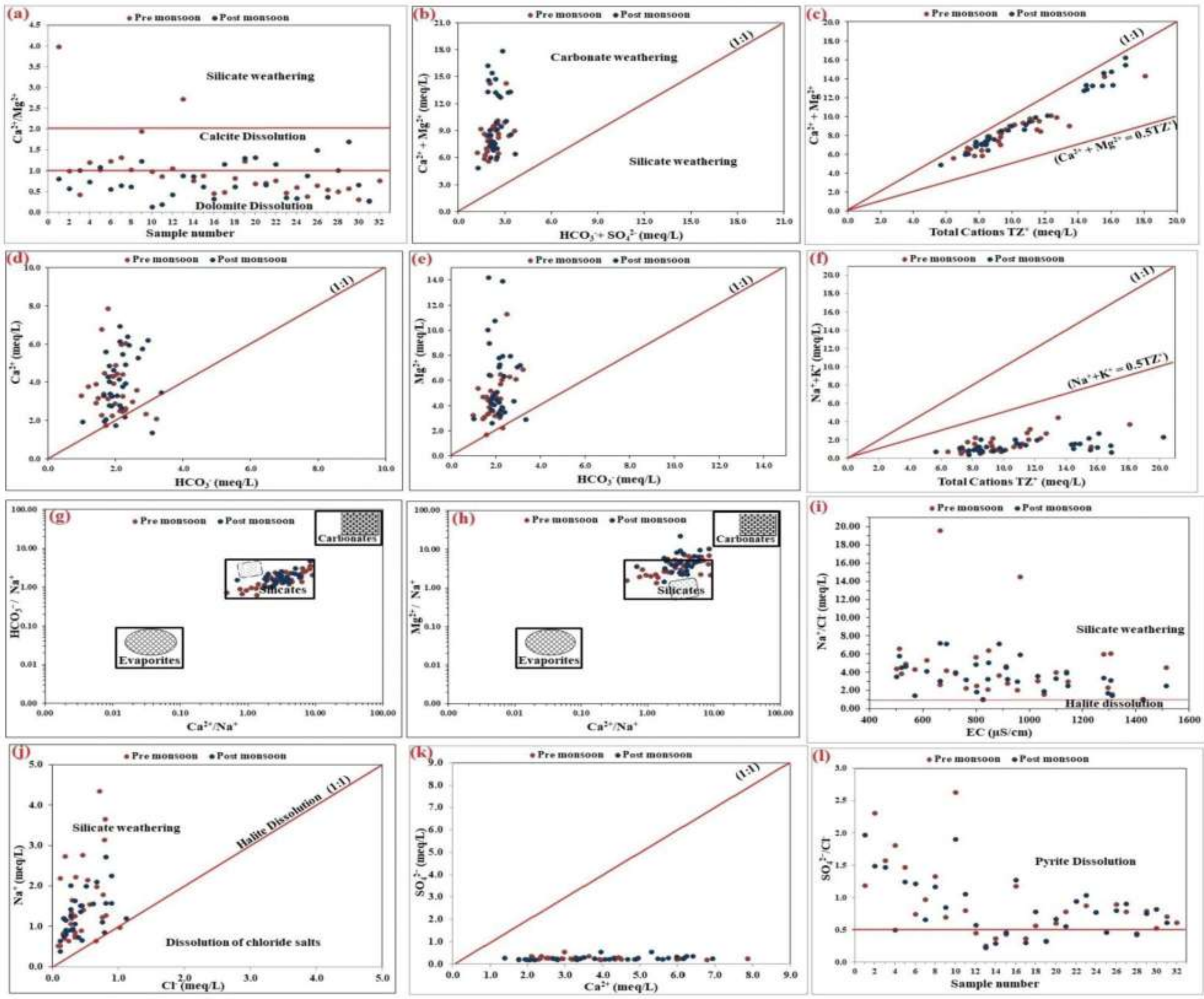


**Figure 5.** Inter-ionic relationship between major ions in groundwater: (a) $Ca^{2+}/Mg^{2+}$, (b) ($Ca^{2+} + Mg^{2+}$ vs. $HCO_3^- + SO_4^{2-}$), (c) ($Ca^{2+} + Mg^{2+}$ vs. total cations $TZ^+$), (d) ($Ca^{2+}$ vs. $HCO_3^-$), (e) ($Mg^{2+}$ vs. $HCO_3^-$), (f) ($Na^+ + K^+$ vs. total cations $TZ^+$), (g) ($Ca^{2+}/Na^+$ vs. $HCO_3^-/Na^+$), (h) ($Ca^{2+}/Na^+$ vs. $Mg^{2+}/Na^+$), (i) ($Na^+/Cl^-$ vs. EC), (j) ($Na^+$ vs. $Cl^-$), (k) ($SO_4^{2-}$ vs. $Ca^{2+}$), and (l) ($SO_4^{2-}/Cl^-$) of the study area.

in above mentioned Equations (11) and (12) may enhance the $Na^+$ content in the groundwater of the study area (Keesari *et al.* 2021, Singh *et al.* 2020b).

$$2NaAlSi_3O_8 + 2H_2CO_3 + 9H_2O \rightarrow Al_2Si_2O_8(OH)_4 + 2Na^{2+} + 4H_4SiO_4 + 2HCO_3^- \quad (13)$$

Further, the end-member plot $HCO_3^-/Na^+$ vs. $Ca^{2+}/Na^+$ (Figure 5(g)) clearly indicates that the silicate weathering processes predominantly drive the aquifer chemistry (Gaillardet *et al.* 1997, Gao *et al.* 2021). The general silicate weathering reaction with carbonic acid is as follow:

$$(Na,K,Ca,Mg)\ silicate + H_2CO_3 \rightarrow H_4SiO_4 + HCO_3^- + Na^+ + K^+ + Ca^{2+} + Mg^{2+} + Clay \quad (14)$$

On the other hand, the plot $Mg^{2+}/Na^+$ vs. $Ca^{2+}/Na^+$ (Figure 5(h)) depicts majority of the groundwater samples are clustered within the silicate zone, and very few samples are scattered in the silicate-carbonate mixing region during the investigational period. This plot clearly shows that silicate mineral is not only the prime source of $Na^+$, $Mg^{2+}$, and $Ca^{2+}$ in the study area. The dissolution of carbonate minerals and reverse ion exchange elevates the contents of alkaline earth elements in groundwater (as expressed in Equations (10–12), (17), and (18). Gao *et al.* (2022) reported that clay minerals, when rich in alluvial sediment, enhance cation exchange processes that affect the cation concentrations in groundwater. The following reactions explain the cation exchange for $Ca^{2+}$ and $Mg^{2+}$ with $Na^+$ in the clay sediments as expressed in Equations (15–18) (Li *et al.* 2018a, 2018b, Zhou *et al.* 2020).

$$Ca^{2+} + 2NaX\ (Clay) \rightarrow 2Na^{+} + CaX_2\ (\text{Ion exchange}) \quad (15)$$

$$Mg^{2+} + 2NaX\ (Clay) \rightarrow 2Na^{+} + MgX_2\ (\text{Ion exchange}) \quad (16)$$

$$2Na^{+} + CaX\ (Clay) \rightarrow 2NaX_2 + Ca^{2+}(\text{Reverse ion exchange}) \quad (17)$$

$$2Na^{+} + MgX\ (Clay) \rightarrow 2NaX_2 + Mg^{2+}(\text{Reverse ion exchange}) \quad (18)$$

The molar $Na^{+}/Cl^{-}$ ratio and bivariate plot $Na^{+}/Cl^{-}$ vs. EC (Figure 5(i)) are prepared to understand the plausible sources of salinity and saline incursions in the study area (Luo *et al.* 2021). The $Na^{+}/Cl^{-}$ ratio varies between 1.0 and 19.6 and 1.1 and 7.2 during pre and post monsoon. All the water samples have molar ratio of $Na^{+}/Cl^{-} > 1$ and $Na^{+}/Cl^{-}$ vs. EC $>1$ for both season. Therefore, $Na^{+}$ ions has other sources than silicate weathering process (weathering of sodic plagioclase mineral as expressed in Equation (13); such as, ion exchange and anthropogenic activities enhance the $Na^{+}$ and $Cl^{-}$ ions relative mobility in groundwater (Marghade 2020). The ratio of $Na^{+}$ vs. $Na^{+}+Cl^{-}$ is $\geq 0.5$ in all the samples during pre monsoon ($0.50-0.95$) and post monsoon ($0.52-0.88$), divulges silicate weathering and ion exchange (as expressed in Equations (14–16)). Further, the plot between $Na^{+}$ vs. $Cl^{-}$ (Figure 5(j)) enables identifying the $Na^{+}$ enrichment in the groundwater of the study area. Majority of the water samples (94 and 100%) during the investigational period fall above the equiline (1:1), elucidating the dominance of $Na^{+}$ over $Cl^{-}$ may be derived from silicate weathering and cation exchange processes along with some anthropogenic inputs (Gao *et al.* 2021, Marghade *et al.* 2021). Few samples (6%) during pre monsoon fall below the equiline 1:1 line suggests the halite dissolution (as expressed in Equation (19) is very limited, thus supports the impact of anthropogenic inputs (Liu *et al.* 2021, Wang *et al.* 2021). Hence, the presence of $Cl^{-}$ in groundwater may be due to industrial discharges, seepage from the septic tanks, and chemical fertilizers application.

$$NaCl \rightarrow Na^{+} + Cl^{-}(\text{Halite dissolution}) \quad (19)$$

The plot of $SO_4^{2-}$ vs. $Ca^{2+}$ indicates the groundwater samples are scattered below the equiline (1:1) for both seasons (Figure 5(k)). The dominance of $Ca^{2+}$ over $SO_4^{2-}$ depicts anhydrite ($CaSO_4$) and gypsum ($CaSO_4 \cdot 2H_2O$) minerals are not the principal source of $Ca^{2+}$ and $SO_4^{2-}$ in the aquifers (Mu *et al.* 2021, Karunanidhi *et al.* 2021b). Therefore, $Ca^{2+}$ and $SO_4^{2-}$ contents in groundwater are originated from different sources in the study area. Moreover, the molar ratio $SO_4^{2-}/Cl^{-}$ is computed to identify the contribution of inorganic sulfide and pyrite ($FeS_2$) dissolution in the groundwater (Chirenje *et al.* 2007). During the investigational period, majority of the samples (81 and 78%) have $SO_4^{2-}/Cl^{-} > 0.5$ (Figure 5(l)), reflecting the oxidation of pyrite minerals and leaching of inorganic sulfide in soil may be the primary source of $SO_4^{2-}$ in the groundwater (Okiongbo and Douglas 2015, Singh *et al.* 2020a). The remaining samples (19 and 22%) during pre and post monsoon have $SO_4^{2-}/Cl^{-} < 0.5$ indicates the influence of anthropogenic inputs on groundwater namely, fertilizers applications, irrigation water seepage, and wastewater discharge (Suthar *et al.* 2009). From the above discussion, it can be inferred that $Ca^{2+}$, $Mg^{2+}$, and $HCO_3^{-}$ are mainly derived from the carbonate and silicate weathering and reverse ion exchange process occurring in the aquifer. On the other hand, the parameters $Na^{+}$, $Cl^{-}$ and $SO_4^{2-}$ are majorly controlled by mixed factors with cation exchange process.

## 4. Pearson correlation matrix (PCM) analysis

Pearson correlation matrix analysis of major ions (Table S2) is employed to understand the inter-ion relationships and extract meaningful information about the various geochemical processes prevailing in the study area aquifer system. The absolute correlation values $0.50-0.75$ and $>0.75$ represent moderate and strong correlation among the ions, respectively (Hossain *et al.* 2020). During pre monsoon, $Mg^{2+}$ have strong positive correlation with $Na^{+}$ ($r=0.67$) and moderately with $SO_4^{2-}$ ($r=0.88$), and for post monsoon, $Ca^{2+}$ show moderately correlation with $Cl^{-}$ ($r=0.67$) and weak correlation with $Na^{+}$ ($r=0.40$) indicates the dissolution of carbonate minerals and reverse ion exchange process impacting the aquifer chemistry (Herojeet *et al.* 2017). $Na^{+}$ have strong positive correlation with $HCO_3^{-}$ (0.76 in pre monsoon and 0.78 in post monsoon), $SO_4^{2-}$ (0.81 in pre monsoon and 0.76 in post monsoon), and moderate positive correlation with $Cl^{-}$ (0.51 in post monsoon). It divulges and supports the role of silicate weathering, limited halite dissolution, ion exchange processes, and anthropogenic inputs, as discussed in above section 3.2. $HCO_3^{-}$ have moderate positive correlation with $SO_4^{2-}$ ($r=0.65$) and $Cl^{-}$ ($r=0.57$) during pre monsoon depicts the presence of sulfate, carbonate, and chloride in the top soil aids the organic matter decomposition process at different levels (El-Shinnawi *et al.* 1974). This process increases the $CO_2$(g) in the upper layer of soil. The percolating water in the soil reacts with $CO_2$(g) forming carbonic acid ($H_2CO_3$) and further breakdown into $HCO_3^-$ in the aquifer system (Raju and Singh 2017). $Cl^-$ exhibits strong positive correlation with $NO_3^-$ (0.86 in pre monsoon) and moderate correlation with $SO_4^{2-}$ (0.55 in pre monsoon and 0.50 in post monsoon) indicates that these ions are originated from similar anthropogenic sources (Khan *et al.* 2021, Liu *et al.* 2021). The relationship of these ions reflects the impact of human activities such as fertilizer use, animal wastes, and farming activity that enrich $SO_4^{2-}$, $Cl^-$, and $NO_3^-$ in the groundwater of the study area (Rao *et al.* 2012, Marghade *et al.* 2021). Further, $SO_4^{2-}$ shows an insignificant correlation with $Ca^{2+}$ (Table S2), indicates that pyrite dissolution and anthropogenic inputs may also be responsible for $SO_4^{2-}$ content in groundwater (Singh *et al.* 2020b, Marghade *et al.* 2021). From the PCM results, it can be concluded that the reverse ion exchange and weathering of aquifer minerals largely controlled $Ca^{2+}$, $Mg^{2+,}$ and $HCO_3^-$ ions concentrations in groundwater. On the other hand, the enrichment of these ions, namely, $Na^+$, $Cl^-$ and $SO_4^{2-}$ are influenced by mixed factors and $NO_3^-$ alone by anthropogenic inputs.

## 5. Dissolution and saturation state of minerals

The results of geochemical profiling (Piper plot, Gibb's diagram, and interionic plots) and PCM clearly indicated that the aquifer chemistry of the study area is mainly influenced by interactions of aquifer materials (minerals-water phases) and cation exchange, except for some ions. Saturation index (*SI*) is computed to ascertain the thermodynamic equilibrium about the dissolution and precipitation state of minerals vis-à-vis the types of water–alluvial interaction (Khan *et al.* 2021, Liu *et al.* 2021). *SI* is the logarithm (base 10) of the ratio of ionic activity product (*IAP*) to mineral solubility product constant ($K_{sp}$) and is evaluated by using Equation (20)

$$SI = \log IAP/K_{sp} \tag{20}$$

The *SI* value $<0$ indicates the mineral in solution is unsaturated, $SI = 0$ (saturation), and *SI* value $>0$ (over saturation) with respect to a particular mineral (Zhang *et al.* 2020, Singh *et al.* 2020b). The *SI* values for seven minerals namely: anhydrite ($CaSO_4$), gypsum ($CaSO_4{:}2H_2O$), halite (NaCl), sylvite (KCl), calcite ($CaCO_3$), dolomite [$CaMg(CO_3)_2$], and aragonite ($CaCO_3$) are extracted and presented in Table S3. The scatter plots of *SI* vs. EC for the groundwater samples are presented in supplementary Figure S2(a–g).

All the groundwater samples have *SI* $<0$ i.e. negative (-) values for anhydrite (-3.16 to $-2.62$ and $-3.39$ to $-2.50$), gypsum (-2.95 to $-2.34$ and $-3.06$ to $-2.17$), halite (-9.02 to $-7.25$ and $-9.0$ to $-7.33$) and sylvite (-9.52 to $-7.94$ and $-9.55$ to $-7.68$) for pre and post monsoon seasons (Table S3). The negative *SI* values for anhydrite and gypsum also corroborate the results of geochemical signatures discussed in section 3.2; thus, dissolution will continue to release $Ca^{2+}$ and $SO_4^{2-}$ ions in the aquifer system. Further, the *SI* values (-) for halite mineral supports the role of restricted dissolution in the contribution of $Na^+$ and $Cl^-$ ions (as discussed in above section 3.2) in the groundwater of the study area. The plots between *SI* vs. EC indicate that anhydrite and gypsum minerals are more influenced in the hydrochemistry due to the faster dissolution process than halite and sylvite [Figure S2(a–d)]. Also, the increasing trend of *SI* values of anhydrite, gypsum, halite, and sylvite along with EC divulges that the dissolution of these minerals in the aquifer system with time may directly lead to groundwater salinity.

Further, the mutual independence between EC and *SI* values infers that the groundwater chemistry has already been affected by the fast dissolution of calcite, dolomite, and aragonite [Figure S2(e–g)]. Calcite *SI* values (-0.45 to 0.95 and $-0.85$ to 0.5) indicate ~43 and ~41% samples are positive (saturated and over saturated) in the total samples for both seasons. Similarly, the *SI* values for dolomite (-0.45 to 2.04 and $-1.09$ to 1.11) infer ~60 and ~72% samples are positive, and aragonite (-0.6 to 0.8 and $-1.99$ to 0.36) show a positive in ~38 and ~13% in the groundwater samples during the investigational period. It appears that the aquifer system has manifested the equilibrium between the aqueous groundwater phase and the carbonate minerals phase, subsequently over saturated leading to precipitation of these minerals. The precipitation of $Ca^{2+}$ and $Mg^{2+}$ makes $HCO_3^-$ the dominant anion and the effective increment of $Na^+$ concentration in the groundwater (Li *et al.* 2018a, b). Moreover, anhydrite, gypsum, halite, and sylvite dissolution may lead to dolomite, calcite, and aragonite sequestration and increase aquifer salinity in the study area (Marghade *et al.* 2021, Karunanidhi *et al.* 2021a).

## 6. Human health risk assessment

### 6.1. Average daily dose (ADD)

The estimated *ADD* values (mean, median, SD, 5th, and 95th percentile) using deterministic and probabilistic methods for the target subpopulation category through ingestion and dermal route are presented in Tables S4 and S5. In the present study, deterministic and probabilistic risk analysis used the 5th and 95th percentile as their lower and upper values estimated for different models. The calculated mean, 5th and 95th percentile $ADD_{ingestion}$ values of $F^-$ and $NO_3^-$ using deterministic and probabilistic methods for the pre and post monsoon seasons are pretty the same for all population groups (Table S4).

The range of variation for $ADD_{dermal}$ values estimated by the deterministic method is higher than the probabilistic technique for both seasons (Table S5). For instance, the deterministically calculated mean, 5th and 95th percentile $ADD_{dermal}$ values for $F^-$ are $\sim$7, $\sim$9, and $\sim$5 higher than the probabilistic method for both seasons. The $ADD_{dermal}$ point estimate for $NO_3^-$ indicates a similar range of mean and 95th percentile, i.e. $\sim$7 and $\sim$6 times higher than the probabilistic approach for both seasons. The 5th percentile $ADD_{dermal}$ of $NO_3^-$ divulges deterministic variation $\sim$8 (pre monsoon) and $\sim$18 (post monsoon) times higher than the probabilistic approach. Further, the comparative study within deterministic (pre monsoon vs. post monsoon) and probabilistic (pre monsoon vs. post monsoon) values reveal that 5th percentile and 95th percentile $ADD_{ingestion}$ and $ADD_{dermal}$ for $F^-$ parameter for both seasons indicate no significant variation. On the contrary, the probabilistically (pre monsoon vs. post monsoon) and deterministically (pre monsoon vs. post monsoon) estimated 95th percentile $ADD_{ingestion}$ and $ADD_{dermal}$ for $NO_3^-$ during pre monsoon show $\sim$3 and $\sim$2 times and 5th percentile values as $\sim$14 and $\sim$6 times higher than the post monsoon values for all subpopulation groups. This may be due to pre monsoon $NO_3^-$ concentration levels $\sim$4 times higher than post monsoon, thus crediting the *ADD* ingestion and dermal contact values more than $F^-$ in both risk estimate models.

### 6.2. Hazard quotient

Deterministic and probabilistic *HQ* estimation for $F^-$ and $NO_3^-$ through ingestion and dermal contact of groundwater is shown in Tables S6 and S7. The mean *HQ* values of $F^-$ and $NO_3^-$ for ingestion and dermal exposure route are below the acceptable limit, i.e. $HQs < 1$ for each subpopulation group. Risk certainty level (*RCL*) is assessed to generate the likelihood percentage scenarios of hazard risk above the threshold value ($HQs > 1$) from all the datasets of particular pathway on the target subpopulations. It is another advantage to determine the *RCL* value in health risk assessment for any exposure pathway even if their mean, 5th, and 95th percentile are below their threshold limit. During pre monsoon, the deterministic estimate through $F^-$ ingestion indicates 3.13% *RCL* in infants and children, respectively. Probabilistic *RCL* related to groundwater ingestion of $F^-$, only infants (2.58%) have a higher risk of non-carcinogenic effect ($HQs > 1$) as compared to other groups like children (0.44%), teens (0.07%), and adults (0.04%) show minimal health impact (Table S6). For post monsoon, deterministic *RCL* confirm no adverse health on the subpopulation groups, whereas probabilistic *RCL* depict the non-carcinogenic health effect on infants (1.51%) and children (0.04%) through $F^-$ ingestion of groundwater.

The $HQ_{ingestion}$ of $NO_3^-$ signify non-cancer health impact at different *RCLs* on target groups from deterministic results (infants: 31.25%; children: 15.63%; teens: 6.25% and adults: 6.25%) more than probabilistic estimates (infants: 23.72%; children: 7.66%; teens: 0.77% and adults: 0.48%) for pre monsoon (Table S6). During post monsoon, deterministic *RCL* shows the only potential threat to infants (3.13%), whereas probabilistic *RCL* refers to infants (1.65%) and children (0.18%) groups that pose a health risk due to groundwater ingestion containing $NO_3^-$ (Table S6). The *HQ RCLs* dermal pathway of chemical parameters ($F^-$ and $NO_3^-$) indicate no possible health risk on the specified subpopulation groups from both approaches (Table S7). Among the analyzed human exposure routes, the ingestion pathway is more profound in health risk from *RCL* results, and the $NO_3^-$ parameter is the key risk indicator for infants and children. For example, the *RCL* ratio of deterministic ($NO_3^-$) vs. deterministic ($F^-$) and probabilistic ($NO_3^-$) vs. probabilistic ($F^-$), their magnitude values range from 1–9.98 and 1–9.21, respectively, thus confirm that $NO_3^-$ is the prominent ion inducing the plausible risk factor.

Further, the ratios of deterministic vs. probabilistic mean $HQ_{ingestion}$ values ($F^-$ and $NO_3^-$) for infants, children, teens, and adults vary from 1.12 to 1.23, 1.13 to 1.16, 1.17 to 1.22, and 1.34 to 1.38, respectively, during the investigational period. Also, the range of deterministic vs. probabilistic ratio of 5th and 95th percentile $HQ_{ingestion}$ values ($F^-$ and $NO_3^-$) for infants ($1.57 - 3.90$ and $0.76 - 1.16$), children ($1.27 - 3.03$ and $0.86 - 1.27$), teens ($1.27 - 3.28$ and $0.93 - 1.33$), and adults ($1.42 - 3.63$ and $1.07 - 1.53$) for both seasons. This range variability of *HQ* values indicates that deterministically estimated values are higher than probabilistically assessed values for the entire subpopulation groups. The above analysis divulges that the deterministic method estimate is based on the extreme value of the input variables, leading to overestimating the output results.

### *6.3. Hazard index and total hazard index*

The non-carcinogenic *HI* associated with groundwater ingestion and dermal contact are presented in Table S8. The pre monsoon mean $HI_{ingestion}$ value exceeds the safety reference level ($HI > 1$) only on the infants' group indicating minor population is more vulnerable in the target subpopulation groups (Figure S3a). In contrast, the post monsoon $HI_{ingestion}$ mean values of all different groups are below the threshold limit (Figure S3a). However, the *RCL*s of deterministic and probabilistic estimates above the acceptable value ($HI_{ingestion} > 1$) for pre monsoon season are as follows: infants (59.38 and 39.60%), children (15.63 and 15.84%), teens (6.25 and 2.72%), and adults (6.25 and 1.87%) (Table S8). For post monsoon season, the significant *RCL* for the deterministic study is only reflected on infants (9.38%), whereas the probabilistic *RCL* results reflect on infants (6.57%) and children (0.58%) as more susceptible groups to health risk than the remaining populations (Table S8). The $HI_{dermal}$ mean, 5th, and 95th percentile values are less than unity and is observed as no threat to the target population groups due to insignificant *RCL* (Table S8 and Figure S3b). Ji *et al.* (2020) from their study in Guanzhong plain, China, also reported that the non-carcinogenic $HI_{oral}$ ($F^-$ and $NO_3$–N) from the chlorinated water and terminal tap water are higher on children than that of adults during dry and wet seasons. The present study conclude that *HQ* and *HI* ingestion pathways have more potential human health risks than that of dermal contacts. Liu *et al.* (2022) got similar findings of non-cancerous health risks from the groundwater of Weining plain, China.

Total hazard index (THI) is the combination of non-carcinogenic hazard risk factors of $F^-$ and $NO_3^-$ through multi-exposure pathways (ingestion and dermal) of groundwater, as shown in Table 4. For pre monsoon, the deterministic *RCL* values indicate that infants are $3.8 - 9.5$ times more susceptible to risk than remaining groups, and children show 2.5 times more risk threat than teens and adults. The probabilistic *RCL* estimates specify that infants are $2.5 - 20.9$ times higher non-cancer risk than children, teens, and adults, children ($5.8 - 8.3$ times) than teens and adults and teens (1.4 times) than adults. During post monsoon, only infants are marked highest *RCL* i.e. 9.38 times than the remaining population groups from deterministic results. On the contrary, probabilistic *RCL* results show

**Table 4.** Statistical description of deterministically and probabilistically calculated total hazard index (*THI*) for ingestion and dermal pathways at different age groups.

| | | Deterministic value | | | | | Risk certainty level (%) | Probabilistic value | | | | | Risk certainty level (%) |
|---|---|---|---|---|---|---|---|---|---|---|---|---|---|
| Age group | THI | Mean | Median | Stdev. | 5% | 95% | THI >1 | Mean | Median | Stdev. | 5% | 95% | THI >1 |
| Infant | Pre monsoon | 1.16E + 00 | 1.15E + 00 | 7.12E-01 | 3.14E-01 | 2.16E + 00 | 59.38% | 1.03E + 00 | 8.41E-01 | 1.73E + 00 | 2.75E-01 | 2.39E + 00 | 39.62 |
| Children | | 7.51E-01 | 7.44E-01 | 4.61E-01 | 2.04E-01 | 1.40E + 00 | 15.62% | 6.57E-01 | 5.82E-01 | 1.03E + 00 | 2.07E-01 | 1.36E + 00 | 15.85 |
| Teen | | 5.42E-01 | 5.37E-01 | 3.33E-01 | 1.47E-01 | 1.01E + 00 | 6.25% | 4.49E-01 | 4.08E-01 | 6.87E-01 | 1.44E-01 | 9.10E-01 | 2.73 |
| Adult | | 5.83E-01 | 5.78E-01 | 3.59E-01 | 1.58E-01 | 1.09E + 00 | 6.25% | 4.24E-01 | 3.81E-01 | 6.45E-01 | 1.41E-01 | 8.44E-01 | 1.90 |
| Infant | Post monsoon | 5.18E-01 | 4.26E-01 | 3.01E-01 | 2.19E-01 | 1.16E + 00 | 9.38% | 4.64E-01 | 3.75E-01 | 8.15E-01 | 1.17E-01 | 1.11E + 00 | 6.57 |
| Children | | 3.36E-01 | 2.76E-01 | 1.95E-01 | 1.42E-01 | 7.54E-01 | 0.00% | 2.92E-01 | 2.55E-01 | 4.69E-01 | 8.74E-02 | 6.30E-01 | 0.58 |
| Teen | | 2.42E-01 | 1.99E-01 | 1.41E-01 | 1.03E-01 | 5.44E-01 | 0.00% | 2.04E-01 | 1.77E-01 | 3.23E-01 | 6.50E-02 | 4.32E-01 | 0.00 |
| Adult | | 2.61E-01 | 2.15E-01 | 1.52E-01 | 1.10E-01 | 5.86E-01 | 0.00% | 1.89E-01 | 1.67E-01 | 2.96E-01 | 6.08E-02 | 3.94E-01 | 0.00 |

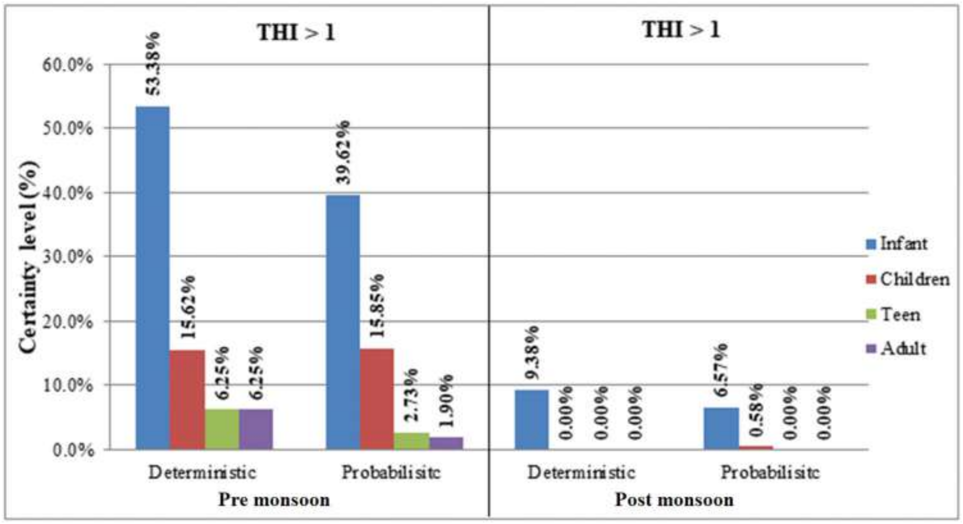


**Figure 6.** Deterministic and probabilistic results of risk certainty level for different population group.

that infants (0.6 − 11.3 times) are more vulnerable than the other population groups and children (0.6 times) more than teens and adults, which is unable to predict by the point estimation method. Therefore, it is noteworthy that the probabilistic simulation method appraises the holistically credible risk scenarios on target subpopulations that may be limited by the deterministic method. Liu *et al.* (2022) suggest that the health risk assessment in groundwater through probabilistic simulation provides comprehensive results than that of deterministic method in different age groups in China. The overall non-carcinogenic health risks in the different population groups are higher in pre monsoon season as compared to post monsoon period due to higher concentration of $NO_3^-$. The present study ascertain that minor populations (infants and children) are more vulnerable to non-carcinogenic risks than those of teens and adults (Figure 6). This is because minor populations show higher sensitivity and poor resilience to withstand the harmful contaminants due to lower body weights. Similar studies on the non-carcinogenic health risks in different population groups elsewhere too report that infants and children are susceptible high risk than those of teens and adults. Examples are: Baqiao District, China (Guo *et al.* 2022), Muktsar district, Punjab, India (Sangwan *et al.* 2021), Jalandhar district, Punjab (Singh *et al.* 2020a), surface water in Taizhou city, Zhejiang Province, China (Zhang *et al.* 2022) and water supply reservoirs in Taizhou City, East China (Yin *et al.* 2021).

### *6.4. Sensitivity and uncertainty analysis*

Sensitivity analysis is employed using the MCS approach to evaluate the input variables that significantly influenced non-carcinogenic risk prediction. The outcome of sensitivity analysis is presented as tornado plots elucidating the Spearman rank-order correlation coefficient in the percentage scale [Figure 7(a,b,c,&d)]. The results of sensitivity analysis for non-carcinogenic $HQ_{ingestion}$ confirmed that respective parameter concentration ($C_M$) is the most precedence variable, followed by exposure frequency (EF) and ingestion rate (IR) of groundwater with a minor contribution in children, teens, and adults for both seasons [Figure 7(a&b)]. On the other hand, the sensitivity analysis shows the order of significant variables as $C_M$, IR, and EF for infants $HQ_{ingestion}$ due to high dependence on water-based liquid diet and less surface area of the body [Figure 7(a&b)]. The non-cancer $HQ_{demal}$ sensitivity analysis outputs reveal the highly significant variables as $C_M$, and minor influence by EF, and exposure time (ET). In contrast, surface area (SA) indicates neutral contribution in any specific population groups during the investigational period [Figure 7(c&d)]. However, Body weight (BW) had a negative inference on non-carcinogenic *HQ* risk simulation through ingestion and dermal pathways in target population groups.

Uncertainty analysis is crucial to determining the conservatism, ramification, and certainty accuracy level of the risk analysis results (Zhang *et al.* 2019). In this study, the application of MCS is notably enhanced to identify the uncertainties quantification in the non-cancer health risk assessment. Nevertheless, there are still other uncertainties that remain unaccounted in the model input variables, thereby limiting the validity of the whole scenario study. For example, (i) the daily water intake and dermal contact of target population groups are not measured during the groundwater

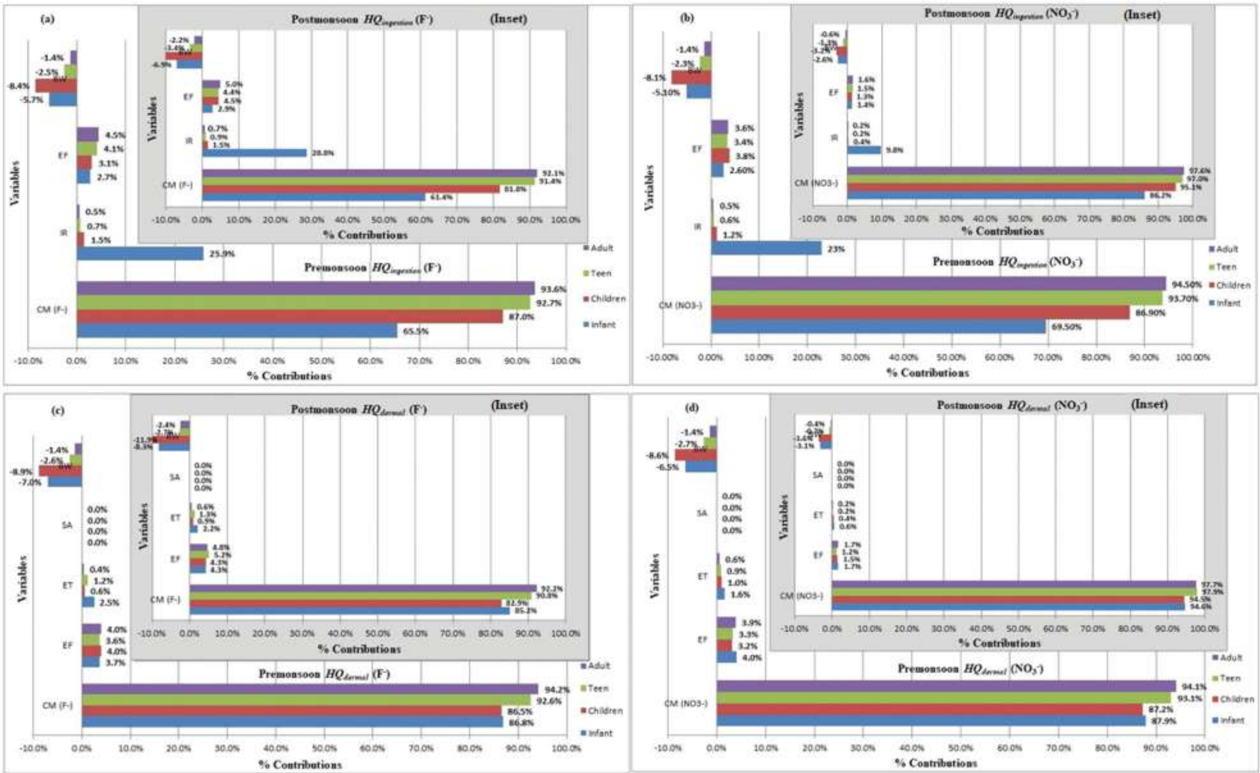


**Figure 7.** (a, b, c, & d) Tornado plot illustrating sensitivity analysis of input variables to the non-carcinogenic *HQ* of groundwater (a & b) pre monsoon and post monsoon (inset) of $F^-$ and $NO_3^-$ ingestion and (c & d) for dermal contact.

sampling, (ii) body weight of the local population are not evaluated, instead used the representative data of the Indian Council of Medical Research (ICMR) and USEPA, (iii) exposure duration, average time, dermal permeability and conversion factor are considered as the same fixed or similar values for deterministic and probabilistic approach for different subpopulation groups, (iv) the variables data to generate the PDFs using MCS are acquired from the USEPA, and other relevant published works, (v) assuming the specific chemical parameter contents in groundwater are the totally bio-absorbable amount by human body might lead to ambiguity in risk analysis, and (vi) the reference dose (*RfD*) for ingestion and dermal are obtained from USEPA. The present findings shall be considered reliable information of HHRA in the target subpopulation groups in the study area compared to reliance on classification based on their parameter concentrations and prescribed National standards.

## 7. Conclusion

This paper highlights groundwater evolution and geochemical profiling using various graphical interpolations, statistical techniques along with quality assessment for drinking purposes. Further, the comparative evaluations of deterministic and probabilistic approaches are applied to determine the non-carcinogenic HHRA for $F^-$ and $NO_3^-$ through ingestion and dermal pathways. This study profoundly conveyed that the health risk may persist in vulnerable groups, even if health concern parameters concentrations are below their respective guideline limits. Major findings of the present study are as under:

- Concentrations of pH, EC, TH, and $Mg^{2+}$ exceed their respective permissible limit at some sites, and ~50% of samples for TDS, TH, $Mg^{2+}$, and $Ca^{2+}$ surpassed the acceptable limit that needs to be cautious and requires necessary treatment. The parameters such as, EC, TDS and $Na^+$ have higher mean values during pre monsoon season indicating enhanced ion exchange processes for mineralization and salinity in aquifers. On the other hand, TH, $Ca^{2+}$, $Mg^{2+}$ and $HCO_3^-$ show elevated mean concentrations during post monsoon season reflecting dissolution of the carbonate and silicate minerals in the percolating rainwater and inverse ion exchange processes in the alluvial aquifers.
- Aquifer chemistry is mainly controlled by water-alluvial interaction and predominant $Ca^{2+}$-$Mg^{2+}$-$HCO_3^-$ water type. Interionic plots corroborated by PCM that $Mg^{2+}$, $Ca^{2+}$, and $HCO_3^-$ are influenced by weathering of aquifer minerals, and $Na^+$, $K^+$, $Cl^+$,

and $SO_4^{2-}$ by mixed factors. Further, the thermodynamic equilibrium of calcite, dolomite, and aragonite with aqueous phase confirmed their major influenced in aquifer chemistry.

- Deterministically and probabilistically estimated $HQ_{ingestion}$ and $HI_{ingestion}$ indicate that $NO_3^-$ is the prominent parameter inducing the plausible risk factor than $F^-$ on the local population. Non-cancer risk (*HQ* and *HI)* for dermal route depicts trivial health risks and could be derelict. Therefore, ingestion is the dominant pathway associated with non-carcinogenic health risks. The calculated THI depicts that infants and children are more susceptible to health risk than teens and adults by probabilistic simulation for both seasons. Therefore, the probabilistic method enables the appraisal *RCLs* of *HQ*, *HI,* and THI in the most holistic credible risk scenarios on target subpopulations that may be limited by the deterministic method.

Proper treatment of water prior to use is strongly recommended to safeguard the human health and prevent the vulnerable age groups from being affected by non-cancer risks. Further, implementation of better industrial policies and their strict enforcement shall minimize the spread of water pollution and protect the fragile sub-Himalayan ecosystem from contamination.

## Acknowledgements

The authors wish to thanks the Editor in Chief and two anonymous reviewers for their valuable suggestions and comments to help improve the manuscript. The authors express their sincere thanks to the Chairperson, Department of Environment Studies and Department of Geology (CAS), Panjab University, for enabling necessary laboratory facilities. Also, express special thanks to Mr. B. Umakanta Sharma, Director "CareFusion- India" for providing the technical and equipment supports. This research did not receive any specific grant from funding agencies in the public, commercial, or not-for-profit sectors.

## Disclosure statement

No potential conflict of interest was reported by the author(s).

## Funding

The author(s) reported there is no funding associated with the work featured in this article.

## ORCID

Herojeet Rajkumar http://orcid.org/0000-0002-7656-9127
Pradeep K. Naik http://orcid.org/0000-0001-7576-2980
Gagandeep Singh http://orcid.org/0000-0003-0620-623X
Madhuri Rishi http://orcid.org/0000-0002-0150-5997

## References

Adimalla, N., Li, P., and Qian, H., 2019. Evaluation of groundwater contamination for fluoride and nitrate in semi-arid region of Nirmal Province, South India: a special emphasis on human health risk assessment (HHRA). *Human & ecological risk assessment*, 25 (5), 1107–1124.

Adimalla, N., and Qian, H., 2019. Hydrogeochemistry and fluoride contamination in the hard rock terrain of Central Telangana, India: analyses of its spatial distribution and health risk. *SN applied sciences*, 1, 202. https://doi.org/10.1007/s42452-019-0219-8

Adimalla, N., and Venkatayogi, S., 2017. Mechanism of fluoride enrichment in groundwater of hard rock aquifers in Medak, Telangana State, South India. *Environmental earth sciences*, 76 (1), 45.

Adimalla, N., and Wu, J., 2019. Groundwater quality and associated health risks in a semi-arid region of south India: implication to sustainable groundwater management. *Human & ecological risk assessment*, 25 (1–2), 191–216.

Ali, S., *et al.*, 2021. Health risk assessment due to fluoride exposure from groundwater in rural areas of Agra, India: Monte Carlo simulation. *International journal of environmental science and technology*, 18, 3665–3676. https://doi.org/10.1007/s13762-020-03084-2

APHA (American Public Health Association), 2005. *Standard methods for the examination of water and wastewater.* 21st ed. Washington, DC: American Public Health Association.

Aravinthasamy, P., *et al.*, 2021. Demarcation of groundwater quality domains using GIS for best agricultural practices in the drought-prone Shanmuganadhi River basin of South India. *Environmental Science and pollution research international*, 28 (15), 18423–18435.

Bilgil, H, Department of Mathematics, Aksaray University, Aksaray 68100, Turkey, 2021. New grey forecasting model with its application and computer code. *AIMS Mathematics*, 6 (2), 1497–1514.

BIS (Bureau of Indian Standards), 2012. *Indian standard drinking water specification*, second ed. New Delhi: Indian Standard Institute, 1–18.

Carrey, R., *et al.*, 2021. Combining multi-isotopic and molecular source tracking methods to identify nitrate pollution sources in surface and groundwater. *Water Research*, 188, 116537.

Ceballos, E., *et al.*, 2021. Assessment of human health risk of chromium and nitrate pollution in groundwater and soil of the Matanza-Riachuelo River basin, Argentina. *Exposure and Health*, 13 (3), 323–336.

CGWB (Central Ground Water Board), 2007. *Groundwater information booklet, Solan District, Himachal Pradesh*. Northern Himalayan Region, Dharamshala: Central Groundwater Board, 1–24.

CGWB (Central Ground Water Board), 2008. *Report on groundwater management study Solan District, Himachal*

Pradesh. Northern Himalayan Region, Dharamshala: Central Groundwater Board, 1–72.

CGWB (Central Ground Water Board), 2018. Aquifer mapping and management of ground water resources, Nalagarh Valley, District Solan, Himachal Pradesh, Northern Himalayan Region, Dharamshala: Central Groundwater Board, 1–73.

CGWB, 2013. *Technical series: E, ground water information booklet*. Solan District, Himachal Pradesh: Ministry of Water Resources, Government of India, 1–18.

Chirenje, T., *et al.*, 2007. Water quality issues in the outer coastal plains New Jersy. In: Sarkar, *et al.*, eds. *Developments in environmental science*, Elsevier, 5, 561–589.

Dolma, K., Rishi, M.S., and Herojeet, R., 2015. Baseline study of drinking water quality– a case of Leh Town, Ladakh (J&K), India. *Hydrology current research*, 6, 198. https://doi.org/10.4172/2157-7587.1000198

Elisante, E., and Muzuka, A.N.N., 2017. Occurrence of nitrate in Tanzanian groundwater aquifers: a review. *Applied water science*, 7 (1), 71–87.

El-Shinnawi, M.M., Shaaban, K.A., and Omran, M.S., 1974. Effect of the co-ion of sulphate, chloride, and carbonate on the decomposition of organic matter in soil. *Zentralblatt Für Bakteriologie, Parasitenkunde, Infektionskrankheiten Und Hygiene. Zweite Naturwissenschaftliche Abteilung: Allgemeine, Landwirtschaftliche Und Technische Mikrobiologie*, 129 (6), 559–564.

Emenike, P.G.C., *et al.*, 2019. Probabilistic risk assessment and spatial distribution of potentially toxic elements in groundwater sources in Southwestern Nigeria. *Science reports*, 9 (1), 15920.

EPA (Environmental Protection Agency), 1993. *Wellhead protection: a guide for small communities*. Washington: Office of Research and Development Office of Water.

Fabro, A.Y.R., *et al.*, 2015. Spatial distribution of nitrate health risk associated with groundwater use as drinking water in Merida, Mexico. *Applied geography*, 6, 49–57.

Feng, W., *et al.*, 2020. Distribution of nitrate content in groundwater and evaluation of potential health risks: a case study of rural areas in northern China. *International journal of environmental research and public health*, 17 (24), 9390.

Freeze, R.A., and Cherry, J.A., 1979. *Groundwater*. Englewood Cliffs: Prentice-Hall.

Gaillardet, J., *et al.*, 1997. Chemical and physical denudation in the Amazon River Basin. *Chemical Geology.*, 142 (3–4), 141–173.

Ganyaglo, S.Y., *et al.*, 2019. Groundwater fluoride contamination and probabilistic health risk assessment in fluoride endemic areas of the Upper East Region, Ghana. *Chemosphere*, 233, 862–872.

Gao, Y., *et al.*, 2022. Hydrogeochemical characteristics and processes of groundwater in an over 2260 year irrigation district: a comparison between irrigated and nonirrigated areas. *Journal of hydrology*, 606, 127437.

Gao, Z., *et al.*, 2021. Assessment of the water quality of groundwater in Bohai Rim and the controlling factors-a case study of northern Shandong Peninsula, north China. *Environmental pollution*, 285, 117482.

Ghaderpoori, M., *et al.*, 2018. Heavy metals analysis and quality assessment in drinking water-Khorramabad city, Iran. *Data in brief*, 16, 658–692.

Gibbs, R.J., 1970. Mechanisms controlling world water chemistry. *Science*, 170 (3962), 1088–1090.

Giri, S., Singh, A.K., and Mahato, M.K., 2020. Monte Carlo simulation-based probabilistic health risk assessment of metals in groundwater via ingestion pathway in the mining areas of Singhbhum copper belt, India. *International journal of environmental health research*, 30 (4), 447–460.

Gleeson, T., *et al.*, 2012. Water balance of global aquifers revealed by groundwater footprint. *Nature*, 488 (7410), 197–200.

GoHP (Government of Himachal Pradesh), 2012. *Annual administration report 2011–2012*. Government of Himachal Pradesh: Industries Department, 1–154.

Guleria, A., and Chakma, S., 2021. Probabilistic human health risk assessment of groundwater contamination due to metal leaching: a case study of Indian dumping sites. *Human & ecological risk assessment.*, 27 (1), 101–133.

Guo, Y., *et al.*, 2022. Groundwater quality in and around a landfill in Northwest China: characteristic pollutant identification, health risk assessment, and controlling factor analysis. *Exposure and Health*. https://doi.org/10.1007/s12403-022-00464-6

He, S., *et al.*, 2022a. Identification and apportionment of shallow groundwater nitrate pollution in Weining Plain, northwest China, using hydrochemical indices, nitrate ss isotopes, and the new Bayesian stable isotope mixing model (MixSIAR).* *Environmental pollution*, 298, 118852.

He, S., *et al.*, 2022b. Predictive modeling of groundwater nitrate pollution and evaluating its main impact factors using random forest. *Chemosphere*, 290, 133388.

Herojeet, R.K., *et al.*, 2017. Quality characterization and pollution source identification of surface water using multivariate statistical techniques, Nalagarh Valley, Himachal Pradesh, India. *Applied water science*, 7 (5), 2137–2156.

Herojeet, R.K., *et al.*, 2016. Application of environmetrics statistical models and water quality index for groundwater quality characterization of alluvial aquifer of Nalagarh Valley, Himachal Pradesh, India. *Sustainable water resources management*, 2 (1), 39–53.

Herojeet, R.K., Rishi, S.M., and Sidhu, N., 2013. Hydrochemical characterization, classification and evaluation of groundwater regime in Sirsa watershed, Nalagarh Valley, Himachal Pradesh, India. *Civil and Environmental Research*, 3 (7), 47–57.

Hossain, S.M.S., *et al.*, 2020. Assessing the groundwater quality and health risk: a case study on Setabganj sugar mills limited, Dinajpur, Bangladesh. *Water Science.*, 34 (1), 110–123.

Hounslow, A., 2018. *Water quality data: analysis and interpretation*. Boca Raton: CRC Press.

Huang, J.X., *et al.*, 2011. Spatial distribution pattern analysis of groundwater nitrate nitrogen pollution in Shandong intensive farming regions of China using neural network method. *Mathematical and computer modeling*, 54 (3–4), 995–1004.

Jain, C.K., and Vaid, U., 2018. Assessment of groundwater quality for drinking and irrigation purposes using hydrochemical studies in Nalbari district of Assam India. *Environmental earth sciences*, 77 (6), 254.

Jamal, A., *et al.*, 2019. Distribution and health risk assessment of heavy metals in soil surrounding a lead and zinc smelting plant in Zanjan, Iran. *Human & ecological risk assessment*, 25 (4), 1018–1033.

Ji, Y., *et al.*, 2020. Seasonal variation of drinking water quality and human health risk Assessment in Hancheng City of Guanzhong Plain, China. *Exposure and health*, 12 (3), 469–485.

Kamaldeep, R.M., Kochhar, N., and Ghosh, N., 2011. Impact of industrialization on groundwater quality—a case study of Baddi-Barotiwala industrial belt, district Solan, Himachal Pradesh, India. *Journal of industrial pollution control*, 27 (2), 153–159.

Karunanidhi, D., *et al.*, 2021a. Appraisal of subsurface hydrogeochemical processes in a geologically heterogeneous semi-arid region of south India based on mass transfer and fuzzy comprehensive modeling. *Environmental geochemistry and health*, 43 (2), 1009–1028.

Karunanidhi, D., *et al.*, 2021b. Groundwater quality evolution based on geochemical modeling and aptness testing for ingestion using entropy water quality and total hazard indexes in an urban-industrial area (Tiruppur) of Southern India. *Environmental science and pollution research international*, 28 (15), 18523–18538.

Karunanidhi, D., *et al.*, 2020. Evaluation of non-carcinogenic risks due to fluoride and nitrate contaminations in a groundwater of an urban part (Coimbatore region) of south India. *Environmental monitoring and assessment*, 192 (2), 102.

Keesari, T., *et al.*, 2021. Isotope and hydrochemical systematics of groundwater from a multi-tiered aquifer in the central parts of Indo-Gangetic Plains, India – implications for groundwater sustainability and security. *Science of the Total Environment*, 789, 147860.

Khan, E., 1970. The geology of the area between Chandigarh and Subathu. *Journal of the Paleontological Society of India*, 14, 47–65.

Khan, F., *et al.*, 2021. Impact of hydrogeochemical processes and its evolution in controlling groundwater chemistry along the east coast of Tamil Nadu and Puducherry, India. *Environmental science and pollution research international*, 28 (15), 18567–18588.

Kim, S.H., *et al.*, 2012. Co-contamination of arsenic and fluoride in the groundwater of unconsolidated aquifers under reducing environments. *Chemosphere*, 87 (8), 851–856.

Kumar, D., *et al.*, 2019. Source characterization and human health risk assessment of nitrate in groundwater of middle Gangetic Plain, India. *Arabian journal of geosciences*, 12 (11), 339.

Kumar, P.J.S., and Augustine, C.M., 2021. Entropy-weighted water quality index (EWQI) modeling of groundwater quality and spatial mapping in Uppar Odai Sub-Basin, South India. *Modeling earth systems and environment*, 8, 911–924. https://doi.org/10.1007/s40808-021-01132-5

Lapworth, D.J., *et al.*, 2017. Groundwater quality in the alluvial aquifer system of Northwest India: new evidence of the extent of anthropogenic and geogenic contamination. *The science of the total environment*, 599–600, 1433–1444.

Lee, S.W., *et al.*, 2006. Human risk assessment for heavy metals and As contaminants in the abandoned metal mine area. *Environmental monitoring and assessment*, 119 (1–3), 233–244.

Li, D., *et al.*, 2021. Bioaccumulation and human health risk assessment of trace metals in the freshwater mussel *Cristaria plicata* in Dongting Lake, China. *Journal of Environmental Sciences*, 104, 335–350.

Li, J., *et al.*, 2020. Evaluating spatiotemporal variations of groundwater quality in Northeast Beijing by self-organizing map. *Water*, 12 (5), 1382.

Li, P., *et al.*, 2018a. Groundwater quality assessment for domestic and agricultural purposes in Yan'an City, northwest China: implications to sustainable groundwater quality management on the Loess Plateau. *Environmental earth sciences*, 77 (23), 775.

Li, P., He, X., and Guo, W., 2019b. Spatial groundwater quality and potential health risks due to nitrate ingestion through drinking water: a case study in Yan'an City on the Loess Plateau of northwest China. *Human & ecological risk assessment.*, 25 (1–2), 11–31.

Li, P., *et al.*, 2019a. Occurrence and health implication of fluoride in groundwater of loess aquifer in the Chinese loess plateau: a case study of Tongchuan, Northwest China. *Exposure and health*, 11 (2), 95–107.

Li, P., *et al.*, 2014. Occurrence and hydrogeochemistry of fluoride in shallow alluvial aquifer of Weihe River. *Environmental earth sciences*, 71 (7), 3133–3145.

Li, X., *et al.*, 2018b. Groundwater chemistry regulated by hydrochemical processes and geological structures: a case study in Tongchuan, China. *Water*, 10 (3), 338.

Lin, M.L., Gui, H.R., and Peng, W.H., 2016. Health risk assessment of heavy metals in the groundwater of a coal mining area in northern Anhui province, China. *Nature environment and pollution technology*, 15, 11–18.

Liu, J., *et al.*, 2021. An investigation into the hydrochemistry, quality and risk to human health of groundwater in the central region of Shandong Province, North China. *Journal of cleaner production*, 282, 125416.

Liu, L., *et al.*, 2022. Occurrence and distribution of groundwater fluoride and manganese in the Weining Plain (China) and their probabilistic health risk quantification. *Exposure and health*, 14, 263–279. https://doi.org/10.1007/s12403-021-00434-4

Luo, Y., *et al.*, 2021. Groundwater geochemical signatures and implication for sustainable development in a typical endorheic watershed on Tibetan plateau. *Environmental science and pollution research*, 28 (35), 48312–48329.

Luo, X.S., *et al.*, 2012. Incorporating bioaccessibility into human health risk assessments of heavy metals in urban park soils. *The science of the total environment*, 424, 88–96.

Ma, Y., *et al.*, 2016. Human health risk assessment of heavy metals in urban stormwater. *Science of the total environment.*, 557–558, 764–772.

Madhav, S., *et al.*, 2018. Geochemical assessment of groundwater quality for its suitability for drinking and irrigation purpose in rural areas of Sant Ravidas Nagar (Bhadohi), Uttar Pradesh. *Geology, ecology, and landscapes*, 2 (2), 127–136.

Marghade, D., *et al.*, 2021. Hydrogeochemical evaluation, suitability, and health risk assessment of groundwater in the watershed of Godavari basin, Maharashtra, Central India. *Environmental science and pollution research international*, 28 (15), 18471–18494.

Marghade, D., 2020. Detailed geochemical assessment & indexing of shallow groundwater resources in metropolitan city of Nagpur (western Maharashtra, India) with potential health risk assessment of nitrate enriched groundwater for sustainable development. *Geochemistry*, 80 (4), 125627.

Mayo, A.L., and Loucks, M.D., 1995. Solute and isotopic geochemistry and ground water flow in the central Wasatch Range, Utah. *Journal of hydrology*, 172 (1–4), 31–59.

Minet, E.P., *et al.*, 2017. Combining stable isotopes with contamination indicators: a method for improved investigation of nitrate sources and dynamics in aquifers with mixed nitrogen inputs. *Water research*, 124, 85–96.

Mu, W., *et al.*, 2021. Hydrochemical and environmental isotope characteristics of groundwater in the Hongjiannao Lake Basin, Northwestern China. *Environmental earth sciences*, 80 (2), 51.

Naik, P.K., *et al.*, 2008. Impact of urbanization on the groundwater regime in a fast growing city in central India. *Environmental monitoring and assessment*, 146 (1–3), 339–373.

Narsimha, A., and Rajitha, S., 2018. Spatial distribution and seasonal variation in fluoride enrichment in groundwater and its associated human health risk assessment in Telangana State, South India. *Human & ecological risk assessment*, 24 (8), 2119–2132.

Okiongbo, K.S., and Douglas, R.K., 2015. Evaluation of major factors influencing the geochemistry of groundwater using graphical and multivariate statistical methods in Yengoa city. *Applied water science*, 5 (1), 27–37.

Piper, A.M., 1944. A graphic procedure in the geochemical interpretation of water-analyses. *Transactions, American geophysical union*, 25 (6), 914.

Qiu, H., and Gui, H., 2019. Heavy metals contamination in shallow groundwater of a coal-mining district and a probabilistic assessment of its human health risk. *Human & ecological risk assessment.*, 25 (3), 548–563.

Radfard, M., *et al.*, 2019. Health risk assessment to fluoride and nitrate in drinking water of rural residents living in the Bardaskan city, arid region, Southeastern Iran. *Desalination and water treatment*, 145, 249–256.

Rahmati, O., *et al.*, 2015. Assessment of the contribution of N-fertilizers to nitrate pollution of groundwater in western Iran (case study: Ghorveh–Dehgelan aquifer). *Water quality, exposure and health*, 7 (2), 143–151.

Rai, S. N., 2003. Groundwater pollution in India- an overview. New Delhi, India: Allied Publishers Pvt. Ltd, 419–436.

Rajasekhar, B., Nambi, I.M., and Govindarajan, S.K., 2018. Human health risk assessment of ground water contaminated with petroleum PAHs using Monte Carlo simulations: a case study of an Indian metropolitan city. *Journal of Environmental Management*, 205, 183–191.

Rajkumar, H., Naik, P.K., and Rishi, M.S., 2019. Evaluation of heavy metal contamination in soil using geochemical indexing approaches and chemometric techniques. *International Journal of Environmental science and technology*, 16 (11), 7467–7486.

Rajkumar, H., Naik, P.K., and Rishi, M.S., 2020. A new indexing approach for evaluating heavy metal contamination in groundwater. *Chemosphere*, 245, 125598.

Raju, A., and Singh, A., 2017. Assessment of groundwater quality and mapping human health risk in central Ganga Alluvial Plain, Northern India. *Environmental processes*, 4 (2), 375–397.

Rao, N.S., Dinakar, A., and Kumari, B.K., 2021. Appraisal of vulnerable zones of non-cancer-causing health risks associated with exposure of nitrate and fluoride in groundwater from a rural part of India. *Environmental research*, 202, 111674.

Rao, N.S., *et al.*, 2012. Chemical characteristics of groundwater and assessment of groundwater quality in Varaha River basin, Visakhapatnam District, Andhra Pradesh, India. *Environmental monitoring and assessment*, 184 (8), 5189–5214.

Rao, N.S., 2017. Controlling factors of fluoride in groundwater in a part of South India. *Arabian journal of geoscience*, 10, 524. https://doi.org/10.1007/s12517-017-3291-7

Saha, N., *et al.*, 2017. Industrial metal pollution in water and probabilistic assessment of human health risk. *Journal of environmental management*, 185, 70–78.

Sangwan, P., Rishi, M.S., and Singh, G., 2021. Assessment of drinking water quality and non-carcinogenic health risk associated with the feed and treated water of water treatment devices (WTDs) in southwest Punjab, India. *Toxicological review*, 41 (2), 536–550. https://doi.org/10.1080/15569543.2021.1906707

Sawyer, G.N., and McCarthy, D.L., 1967. *Chemistry of sanitary engineers*. 2nd ed. New York: McGraw Hill, 518.

Selvam, S., *et al.*, 2021. Assessment of groundwater from an industrial coastal area of south India for human health risk from consumption and irrigation suitability. *Environmental research*, 200, 111461.

Sidhu, N., Rishi, M.S., and Herojeet, R.K., 2013. Groundwater quality variation with respect to aquifer dispositioning in urbanized watershed of Chandigarh, India. *International journal of environment, ecology, family and urban studies*, 3 (2), 87–98.

Singh, G., Rishi, M.S., and Arora, N.K., 2019. Integrated GIS-based modelling approach for irrigation water quality suitability zonation in parts of Satluj River Basin, Bist Doab region, North India. *SN applied sciences*, 1, 1438.

Singh, G., *et al.*, 2020a. Multivariate analysis and geochemical signatures of groundwater in the agricultural dominated taluks of Jalandhar district, Punjab, India. *Journal of geochemical exploration*, 208, 106395.

Singh, G., *et al.*, 2020b. Evaluation of groundwater quality and human health risks from fluoride and nitrate in semi-arid region of northern India. *Environmental geochemisty and health*, 42 (7), 1833–1862.

Singh, U.K., and Kumar, B., 2017. Pathways of heavy metals contamination and associated human health risk in Ajay River basin, India. *Chemosphere*, 174, 183–199.

Skold, A., Cosco, D.L., and Klein, R., 2011. Methemoglobinemia: pathogenesis, diagnosis, and management. *Southern medical journal*, 104 (11), 757–761.

Srinivasamoorthy, K., *et al.*, 2014. Hydrochemical characterization and quality appraisal of groundwater from Pungar sub basin, Tamil Nadu, India. *Journal of King Saud University – science*, 26 (1), 37–52.

Suthar, S., *et al.*, 2009. Nitrate contamination in groundwater of some rural areas of Rajasthan, India. *Journal of hazardous materials*, 171 (1–3), 189–199.

Tiwari, A.K., Singh, A.K., and Mahato, M.K., 2018. Assessment of groundwater quality of Pratapgarh district in India for suitability of drinking purpose using water quality index

(WQI) and GIS technique. *Sustainable water resources management*, 4 (3), 601–616.

USDHAHS (U.S. Department of Health and Human Services), 2017. Toxicological profile for nitrate and nitrate, Agency for Toxic Substances and Disease Registry, the Public Health Service, 1–324. Available from: https://www.atsdr.cdc.gov/toxprofiles/tp204.pdf [Accessed 19 April 2021].

USEPA (U.S. Environmental Protection Agency), 1989. *Risk assessment guidance for superfund volume i. Human health evaluation manual (part A).* Washington, D.C.: U.S. Environmental Protection Agency, Office of Emergency and Remedial Response.

USEPA (U.S. Environmental Protection Agency), 1992. *Guidelines for exposure assessment. Federal register notice 57*. Washington, D.C.: Risk Assessment Forum, U.S. Environmental Protection Agency, 22887–22938.

USEPA (U.S. Environmental Protection Agency), 1997. *Guiding principles for Monte Carlo analysis*. Washington, DC: Risk Assessment Forum, U.S. Environmental Protection Agency, 1–23.

USEPA (U.S. Environmental Protection Agency), 2002a. *A review of the reference dose and reference concentration processes, risk assessment forum.* Washington, DC: U.S. Environmental Protection Agency, 1–192.

USEPA (U.S. Environmental Protection Agency), 2002b. *Supplemental guidance for developing soil screening levels for superfund site*. Washington, DC: Office of Emergency and Remedial Response.

USEPA (U.S. Environmental Protection Agency), 2004. *Risk assessment guidance for superfund (RAGS), vol. I: human health evaluation manual (Part E, supplemental guidance for dermal risk assessment)*. Washington DC: US Environmental Protection Agency.

USEPA (U.S. Environmental Protection Agency), 2011. *Exposure factors handbook ed* (final). Washington DC: US Environmental Protection Agency.

USEPA (U.S. Environmental Protection Agency), 2012. Integrated risk information system. United States Environmental Protection Agency. https://cfpub.epa.gov/ncea/iris/search/index.cfm.

Wang, D., *et al.*, 2020. Finding high-quality groundwater resources to reduce the hydatidosis incidence in the Shiqu County of Sichuan Province, China: analysis, assessment, and management. *Exposure and Health*, 12 (2), 307–322.

Wang S. 2004. *Research and its application on hydrological system fuzzy uncertainly analysis method*. Doctor's Thesis. Dalian University of Technology, Dalian (in Chinese)

Wang, Y., and Li, P., 2022. Appraisal of shallow groundwater quality with human health risk assessment in different seasons in rural areas of the Guanzhong Plain (China). *Environmental Research*, 207, 112210.

Wang, Z., *et al.*, 2021. Hydrochemistry characters and hydrochemical processes under the impact of anthropogenic activity in the Yiyuan city, Northern China. *Environmental earth sciences*, 80 (2), 60.

WHO (World Health Organisation), 2008. *Guidelines for drinking-water quality*. Third edition, incorporating first and second addenda. Geneva: World Health Organisation, 1–668.

WHO (World Health Organization). 2011. *WHO guidelines for drinking water quality*. Fourth ed. Geneva: World Health Organisation, 1–564.

Wongsanit, J., *et al.*, 2015. Contamination of nitrate in groundwater and its potential human health: a case study of lower Mae Klong river basin, Thailand. *Environmental science and pollution research international*, 22 (15), 11504–11512.

Yin, Z., *et al.*, 2021. Water quality characteristics and health risk assessment of main water supply reservoirs in Taizhou City, East China. *Human & ecological risk assessment.*, 27 (8), 2142–2160.

Zhai, Y., *et al.*, 2017. Does the groundwater nitrate pollution in China pose a risk to human health? A critical review of published data. *Environmental science and pollution research international*, 24 (4), 3640–3653.

Zhang, Q., Xu, P., and Qian, H., 2020. Groundwater quality assessment using improved water quality index (WQI) and human health risk (HHR) evaluation in a semi-arid region of Northwest China. *Exposure and health*, 12 (3), 487–500.

Zhang, Y., *et al.*, 2019. Implementation of long-term assessment of human health risk for metal contaminated groundwater: a coupled chemical mass balance and hydrodynamics model. *Ecotoxicology and environmental safety*, 180 (30), 95–105.

Zhang, Y., Wu, J., and Xu, B., 2018. Human health risk assessment of groundwater nitrogen pollution in Jinghui canal irrigation area of the loess region, northwest China. *Environmental earth sciences*, 77 (7), 273.

Zhang, Z., *et al.*, 2022. Surface water quality and health risk assessment in Taizhou City, Zhejiang Province (China). *Exposure and health*, 14 (1), 1–16.

Zhou, Y., *et al.*, 2020. Solute geochemistry and groundwater quality for drinking and irrigation purposes: a case study in Xinle City, North China. *Geochemistry*, 80 (4), 125609.

Zhou Z. 2017. *Study on the vulnerability assessment of dam-break flood disaster considering uncertainty*. Doctor's Thesis. Tianjin University, Tianjin (in Chinese)